

Chapter 6

Superhard and Ultrahard Nanostructured Materials and Coatings

Prof. Dr. Prof. h.c. Dr. h.c. Stan Veprek
and Dr. Maritza G.J. Veprek-Heijman

Abstract The recent search for new super- and ultrahard materials is briefly summarized. It is shown that many materials with high elastic moduli cannot be superhard because, upon finite shear, electronic instabilities and transformations to softer phases occur, particularly in materials which contain metals with d-electrons or non-binding electron pairs. Hardness enhancement can be achieved in nanostructured materials, but it is limited by grain-boundary shear when the crystallite size decreases to 10–15 nm called the “strongest size.” When however, low-energy grain boundaries, such as stacking faults and twins, or one-monolayer thin sharp grain boundaries of silicon nitride strengthened by valence charge transfer are introduced, the grain-boundary shear can be reduced and the “strongest size” shifted to a few nanometers. This results in a significantly increased hardness enhancement. In such a way, extrinsically ultrahard materials, such as nanotwinned nt-c-BN and nt-diamond, and nanocomposites consisting of 3–4 nm small transition metal nitride with about one monolayer silicon nitride interfacial layer with hardness exceeding 100 GPa have been prepared. We discuss the conditions which have to be met for such nanocomposites to be super- and ultrahard and show that not all such systems can be superhard. Impurities, mainly oxygen content of more than a few hundred ppm, are critical limitation for achieving the high hardness. The superhard nanocomposites, such as nc-(Ti_{1-x}Al_x)N/Si₃N₄ and nc-(Cr_{1-x}Al_x)N/Si₃N₄, find important applications as wear-protection coatings on tools for machining, stamping, injection molding, and the like.

Prof. Dr. Prof. h.c. Dr. h.c. S. Veprek (✉)
Professor Emeritus, Department of Chemistry, Technical University Munich,
Munich, Germany
e-mail: Stan.Veprek@lrz.tum.de

Dr. M.G.J. Veprek-Heijman
Department of Chemistry, Technical University Munich, Munich, Germany
e-mail: Maritza.Veprekheijman@lrz.tum.de

1 Introduction

Many efforts have been conducted recently to design new superhard (hardness $H \geq 40$ GPa, c-BN ≈ 48 GPa) and ultrahard ($H \geq 80$ GPa) comparable to diamond (80–100 GPa) materials. The majority of the papers focused on materials with large elastic moduli (“ultra-incompressibility”) which are believed to be “intrinsically” superhard. However, large elastic moduli do not guarantee high hardness, because the moduli describe only the resistance of a material against elastic (reversible) infinitesimal distortion near the equilibrium positions, whereas plastic deformation occurs by shear at large strain at the atomic level. The apparent correlation of the hardness of some material with the shear modulus, G , which however displays large scatter [see Fig. 1 in (Teter 1998)], is due to the fact that the plastic flow, which occurs mainly by multiplication and movement of dislocations, is impeded by a variety of mechanisms (grain boundaries, precipitates, dispersed particles, and the like) that are dependent on G .

One has to keep in mind that the indentation hardness is the average pressure beneath the indenter under conditions of fully developed plasticity, where no single crystal exists anymore, and thus the material is full of flaws (Argon 2008). Therefore the recent theories of “hardness of an ideal crystal” (e.g., Gao et al. 2003; Simunek and Vackar 2006; Simunek 2009) calculate by first principles only the elastic stiffness of the crystals but not their plastic hardness under the condition of fully developed plasticity.

Sufficiently high elastic moduli are of course needed but not sufficient for achieving high hardness, because upon finite shear that occurs at atomic level upon plastic deformation, many materials undergo electronics instabilities and structural transformations into softer phases. For example, C_3N_4 , which has elastic moduli, calculated by first principles, higher than c-BN and close to those of diamond (Cohen 1994; Liu and Cohen 1989; Zhang Y et al. 2006), has hardness less than 30 GPa (Veprek et al. 1995) because upon a shear of 0.24 in the (111) (Argon 2008) slip system, the non-binding electron pairs on nitrogen interact with atomic orbitals of carbon forming double bonds, and the system transforms into a softer, graphite-like phase (Zhang Y et al. 2006).

Rhenium diboride, ReB_2 , like other diborides of 5d metals, has also large elastic moduli but hardness less than 30 GPa (see Chap. 4) because upon shear within the (0001) (Christiansen et al. 1998) slip system, it undergoes a number of electronic instabilities and transformation to instable and metastable phases with lower shear resistance [see Fig. 1 in (Zhang et al. 2010a)]. The formation of a variety of softer phases beneath the indenter is probably also the reason for the slow approach of the measured hardness to the load-invariant value which requires large load of more than 6 newtons (N) [see Fig. 2a in (Chung et al. 2007)]. The valence orbitals of osmium and iridium atoms differ only by one electron in the 5d shell (Os, $4f^{14}5d^66s^2$; Ir, $4f^{14}5d^76s^2$), yet their diborides OsB_2 and IrB_2 display very different plastic deformation paths and hardness (OsB_2 , 30 GPa; IrB_2 , 18 GPa) because of different crystal field splitting instabilities (Zhang et al. 2014). Diamond transforms to graphite

upon shear of > 0.3 in the (111) (Argon 2008) slip system as shown by first-principle calculations (e.g., Veprek et al. 2010) and as experimentally observed by Raman scattering of the indented area (Gogotsi et al. 1999). However, because of the relatively simple electronic structure of carbon, this transformation requires a very high shear stress. Therefore, diamond is intrinsically ultrahard. The electronic instabilities of the 5d orbitals due to the crystal field splitting and instabilities due to non-binding electron pairs upon finite shear are probably general phenomena limiting the hardness of many materials with high elastic moduli.

Boron suboxide, B_6O , has high hardness of 40–45 GPa in spite of its lower elastic moduli as compared with OsB_2 and ReB_2 because it has an electronically stable three-dimensional network of covalent bonds (Zhang et al. 2011). These few examples should be sufficient to illustrate that the search for new intrinsically superhard materials should not focus only on materials with high elastic moduli. Instead, much deeper insight into the electronic structure and its stabilities upon finite shear and into the deformation paths are needed (Veprek 2013).

Interesting is the case of heavily boron-doped diamond BC_5 for which load-invariant Vickers hardness of 71 GPa, higher than that of c-BN, has been reported (Solozhenko et al. 2009), although the ideal shear strength of BC_5 , calculated by means of density functional theory, DFT, was significantly lower than that of c-BN (Zhang et al. 2009). The answer to this puzzle was identified in the small crystallite size of the material of 10–15 nm (Solozhenko et al. 2009) that is in the range of the so-called strongest size (Argon and Yip 2006). Also the high Vickers hardness of c- BC_2N of about 76 GPa (Solozhenko et al. 2001) has been explained by the small size of the nanocrystals (Zhang Y et al. 2004).

With decreasing crystallite size, the strength and hardness of a material increase because the grain boundaries impede the plastic deformation, by the well-known Hall-Petch mechanism for dislocations and by twinning, slip, and other mechanisms of plasticity (Argon 2008). The thickness of the large-angle grain boundaries extends usually over a distance of about 3–4 interatomic bonds. Therefore, below a crystallite size, d , of 10–15 nm, the fraction of the atoms in the grain boundaries strongly increases as $1/d$. The grain boundaries are weaker than the crystals because of density deficit and disorder therein. Therefore, with crystallite size decreasing below about 10 nm, the strengthening is replaced by the grain-boundary shear (also called “sliding” or “inverse Hall-Petch”) below the “strongest size,” and the material softens (Fig. 6.1). This transition from strengthening to softening has been found in many nanosized materials, such as metals (e.g., Argon and Yip 2006; Schiøtz et al. 1998; Schiøtz and Jacobsen 2003; Siegel and Fougere 1995) and ceramics (Skrovanek and Bradt 1979). The crystallite size where the strengthening changes to softening has been called by Yip “the strongest size” (Yip 1998). This strengthening with crystallite size decreasing to about 10–15 nm is found in almost any system when, for example, some elements or impurities are added leading to decomposition of a solid solution into two or more phases and concomitant grain refinement. However, the amount of such strengthening is limited by the grain-boundary shear as shown in Fig. 6.1. The “strongest size” can be slightly shifted to a smaller crystallite size, and the strength and hardness increased when

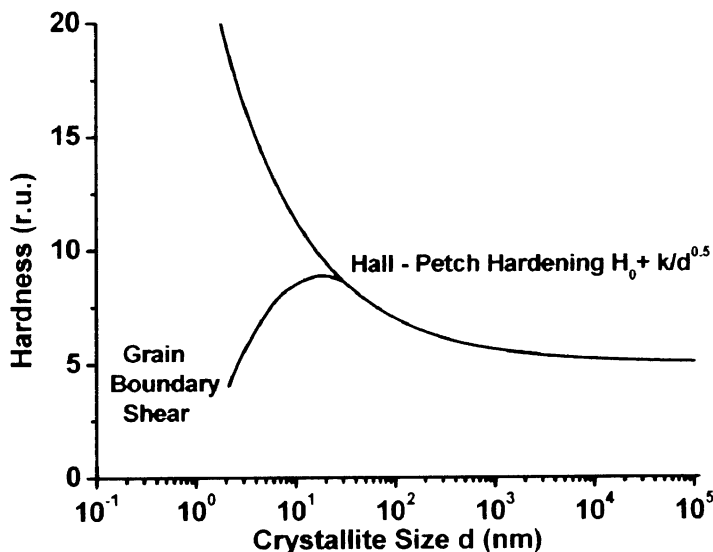


Fig. 6.1 Increase of the strength and hardness due to grain-boundary strengthening with decreasing crystallite size and its weakening due to grain-boundary shear below about 10–20 nm (From Veprek and Veprek-Heijman (2012) with permission)

the grain boundaries are made dense by thermal treatment. However there is a principal limitation to such treatment because the majority of nanosized materials coarsen upon annealing.

The question arises as if this “strongest size” could be shifted to a lower crystallite size by the formation of “strengthened” interfaces so that the “grain-boundary strengthening” would work even at a lower grain size of few nm. This has been the basic idea in the “concept for the design of novel superhard coatings” (Veprek and Reiprich 1995): to choose a quasi-binary or ternary system that will strongly segregate into two or more phases of which the one should form nanocrystals smaller than 10 nm, whereas the other one should form a very thin and sharp interfacial layer. We shall show that this is indeed possible in systems, such as Ti-Si-N, where the solid solution decompose spinodally with large de-mixing energy (Veprek and Veprek-Heijman 2012; Zhang and Veprek 2006). In recent years, this idea has been extended to low-energy interfaces, such as stacking faults (Jian et al. 2013) and twins (Huang et al. 2014; Tian et al. 2013; Xu and Tian 2015). The twins are of a particular interest because there is some evidence that in nanocrystals the dislocation activity upon plastic deformation is replaced by twinning (Zhu et al. 2009).

Of course one will ask what is the smallest crystallite size that can be prepared, and what maximum strength and hardness can be achieved. There is probably no universal answer to it, but some indications can be found in our earlier work on nanocrystalline silicon (nc-Si). It has been shown that there is a lower limit to the crystallite size of about 3 nm, because the tensile strain energy, originating from the

grain boundaries, thermodynamically destabilizes the nc-Si. Therefore amorphous silicon (a-Si) is preferred below that crystallite size because there are no grain boundaries in a-Si (Veprek et al. 1982). Because a similar strain was found in the superhard nc-TiN/Si₃N₄ nanocomposites, a similar effect may explain why the strongest nanocomposites have the size of TiN nanocrystals about 3 nm. We shall discuss this point in Sect. 2.5.

2 Concepts for the Design of New Nanostructured Superhard Materials

2.1 *Heterostructures and Nanolaminates*

Koehler was the first scientist who suggested to design new strong materials on the basis of nanolayered heterostructures (Koehler 1970). The idea was to form alternating layers of different materials with sufficiently different shear moduli but similar lattice constant to form coherent interfaces. The thickness of the individual layers should be small to make sure that the dislocation multiplication source cannot operate. Under stress, a dislocation present in the softer layer with a small shear modulus G_I would move toward the interface with the stronger material where the elastic mirror force would be hindering it to pass. In such a way, the dislocation activity should be impeded by the coherent or semi-coherent interfaces. In a note added in proof, Koehler stated “The ideas described in this note are also valid if one of the materials is amorphous.” Indeed, it has been found later on that the Koehler mechanism of strengthening operates also in polycrystalline nanolaminates and when one of the materials forms amorphous layers (e.g., Hilz and Holleck 1996; Holleck and Schier 1995; Sproul 1994, 1996; Yashar et al. 1999; Yashar and Sproul 1999).

Lehoczky was the first researcher who verified the idea of Koehler experimentally by depositing heterostructures of soft metals (e.g., Al-Cu) and conducting tensile tests. He has shown that, when the thickness of the layers decreased to a few 10 nm, the tensile yield strength of the laminates strongly increased. Although these metallic nanolaminates were not superhard, it is worth mentioning this pioneering work, because this was the first and to the best of our knowledge the only experimental proof of the concept of Koehler in tensile test (Lehoczky 1978a, b). In all following work, only the hardness has been measured.

Superhard heterostructures with hardness exceeding 40 GPa have been prepared when the concept of Koehler has been applied to hard transition metal nitrides. We cannot review here all the papers which have been published on the heterostructures and nanolaminates. Therefore we quote only the first papers from the University of Linköping (Sweden) and Northwestern University (USA) whose scientists pioneered this field (e.g., Helmersson et al. 1987; Mirkarimi et al. 1990, 1994; Hubbard et al. 1992; Shin et al. 1992) and refer to several review articles (Barnett 1993; Yashar and Sproul 1999; Barnett and Madan 1998) for further details.

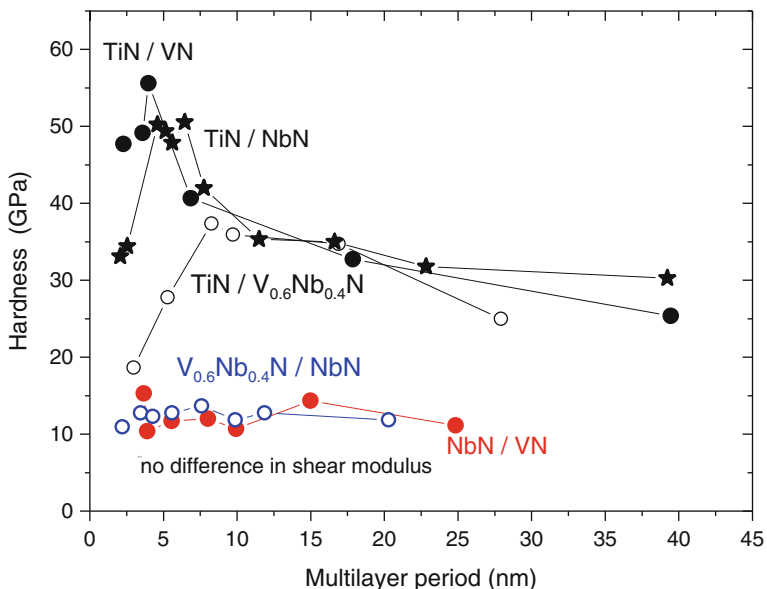


Fig. 6.2 Examples of hardness enhancement in heterostructures with different shear moduli of the pairs (TiN/VN, TiN/NbN, TiN/V_{0.6}Nb_{0.4}N) and with no significant difference in the moduli (NbN/VN, V_{0.6}Nb_{0.4}N)

In Fig. 6.2, we summarize several examples collected from these papers. Heterostructures with pairs of nitrides having different elastic moduli but similar lattice constant (single-crystalline TiN/VN and TiN/V_{0.6}Nb_{0.4}N, polycrystalline TiN/NbN) show pronounced hardness enhancement, whereas heterostructures which have only small difference in elastic moduli (NbN/VN, V_{0.6}Nb_{0.4}N) show no observable hardness enhancement. The decrease of the hardness at smaller multilayer period is due to roughness of the interface (Chu and Barnett 1995). Here we see the importance of sharp interface; we shall come to this point later in Sects. 2.4 and 2.5.

These heterostructures have been deposited by magnetron sputtering from two targets, and the composition has been changed by opening and closing shutters between the targets and the substrate (Barnett 1993). This provided fairly sudden changes from one composition to the other with interfaces whose sharpness has been limited only by ion-impact or thermally induced mixing.

The requirement for a sharp interface might appear a problem when the heterostructures and nanolaminate coatings should be used as wear protection on tools for machining. This is due to the fact that in the industrial coating system, the deposition of the individual layers from different targets occurs continuously, while the tools being coated are fixed on a rotating turntable. Nevertheless, Münz et al. were able to demonstrate that tools such as drills, mills, forming tools, and knives coated with nanolaminates deposited in an industrial coating equipment with large planar targets showed significantly improved cutting performance (Münz et al. 2001).

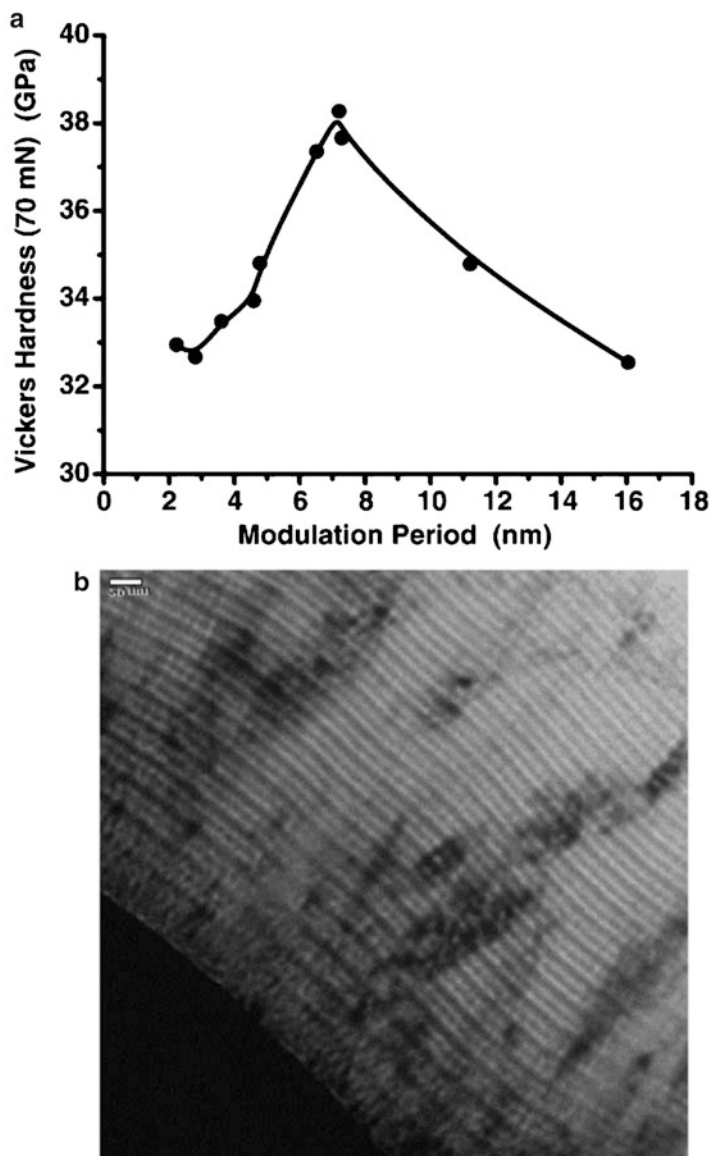


Fig. 6.3 (a) Hardness of the nc-(Ti_{1-x}Al_x)N/Si₃N₄ nanolayered nanocomposite coatings as the function of the period of the compositional modulation, (b) transmission electron micrograph showing the compositional modulation (From Veprek and Veprek-Heijman (2008) with permission)

Since this early development, the hard and superhard heterostructure and nanolaminate coatings are finding many applications, as illustrated, for example, in Fig. 6.3. The nc-(Ti_{1-x}Al_x)N/Si₃N₄ nanocomposite coatings (see Sect. 2.5) are deposited from two cylindrical vacuum arc cathodes consisting of titanium and

Al-Si alloy, which are placed in the center of the industrial coating chamber (for more detail, see www.shm-cz.cz). When the tools being coated are rotating around these cathodes, their composition is modulated being more Ti-rich on the side close to the Ti cathode and more Al + Si-rich on the opposite side. Although in this case no “heterostructures” but only coatings with modulated compositions were deposited, the effect of the hardness enhancement is clearly seen. Moreover, because the modulation of the composition results also in modulation of the elastic moduli, it results in enhancement of the fraction toughness. Coatings with modulated elastic moduli are much more resistant to crack propagation than bulk materials (Matthews et al. 2001).

2.2 *Hardness Enhancement Due to Refinement of the Grain Size*

As discussed in Sect. 1, the enhancement of strength and hardness due to the refinement of the grain size occurs in almost any system, but the hardness enhancement is limited to that corresponding to the “strongest size” of about 10–15 nm. This refinement can be obtained by a variety of means. For example, Barna et al. reported strong refinement of Al films when the aluminum has been deposited by evaporation in poor vacuum so that the films were contaminated by oxygen (Barna and Adamik 1998; Petrov et al. 2003). Depending on the Al:O flux ratio during the deposition, thin or thick Al₂O₃ layer is formed around the Al grains whose size decreased with increasing amount of oxygen down to a few tens of nanometers. Of course this is not a method for the preparation of superhard nanocomposites. This example should only illustrate that grain size refinement occurs in many cases when two immiscible materials form during the deposition.

Many papers have been published during the last 20 years about the preparation of nc-TmN/SiN_x (Tm = Ti, W, V, and many other transition metals) and other nanocomposites where a hardness enhancement has been found. Although, in many cases, these papers provide broad characterization, a systematic study of the hardness enhancement as function of the grain size is missing. However, the present authors found that, whenever enough data is available to extract the information from the papers, the maximum hardness enhancement correlates with the grain size of about 10–15 nm, i.e., with the “strongest size.” For example, in the AlN/SiN_x nanocomposites, the maximum hardness of about 30 GPa [see Fig. 5 in Pélisson et al. (2007)] is achieved at Si content of about 7–13 at.% that corresponds to “AlN” grain size between of about 20 and 5 nm [see Fig. 3 in Pélisson et al. (2007)]. Such nanocomposites are not superhard as those with one monolayer Si₃N₄ interfacial layer which is strengthened by valence charge transfer, to be discussed in Sect. 2.5. Unfortunately, this important difference is neglected in many papers.

Also in the “high-entropy alloys” (Tsai and Yeh 2014), hardness enhancement is often found which might be related to the grain refinement (e.g., Hsieh et al. 2013;

Huang and Yeh 2009). As pointed out recently, high configuration (“mixing”) entropy provides a way to rationalize why a homogeneous solid solution forms (if it forms) in these systems, but it is not a useful a priori predictor if the so-called high-entropy alloy will form thermodynamically stable single-phase solid solutions (Otto et al. 2013). In many cases, positive (destabilizing) mixing enthalpy dominates over the mixing entropy, and the system segregates forming a nanosized composite material. Therefore, much more detailed studies are needed to make sure which effects dominate in a given system.

As mentioned, hardness enhancement by refinement of the grain size is limited to about 30–35 GPa in all the cases where the necessary information is available. Therefore, superhard materials can be formed by the simple grain refinement only when the terminal phases are already very hard, as in the case of nanocrystalline c-BN and c- and wurtzite w-BN nanocomposites reported by Dubrovinskaia et al. (Dubrovinskaia et al. 2007). These researchers prepared the c- and w-BN nanocomposites by high-temperature, high-pressure (HTHP) synthesis and reported high hardness of about 85 GPa, close to the hardness of diamond as shown in Fig. 6.4. One notices that the large increase of the load-invariant hardness of the nanocomposite occurs at crystallite size 13–15 nm, the “strongest size.” Single-phase c-BN shows also an enhancement of hardness at a crystallite size of about 40 nm. Using monomodal pyrolytic graphite with an ideal turbostratic structure, Solozhenko et al. (2012) succeeded to suppress the formation of w-BN and prepare single-phase nanocrystalline c-BN with load-invariant hardness of 85 GPa at crystallite size of 20 nm [see Fig. 3b in (Solozhenko et al. 2012)]. These materials

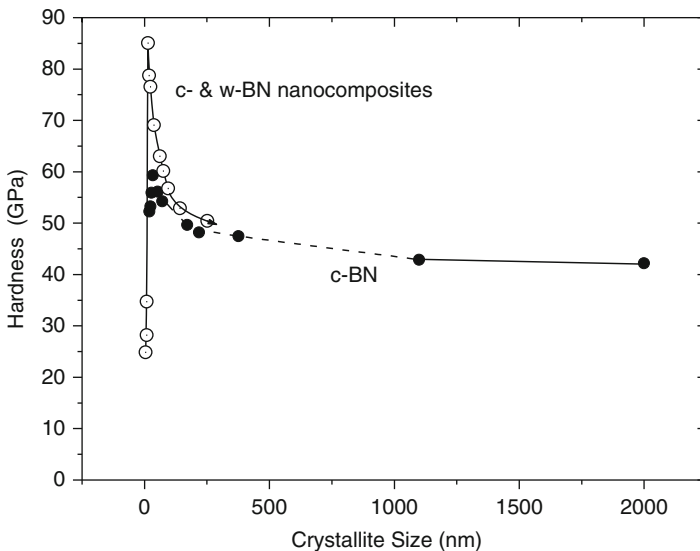


Fig. 6.4 Dependence of the load-invariant hardness on crystallite size in a single-phase c-BN and in nanocomposites consisting of cubic and wurtzite BN (From Dubrovinskaia et al. (2007) with permission)

have been prepared by means of HTHP synthesis that is suitable for the preparation of single crystals and polycrystals, but not coatings on, e.g., tools for machining, which is one of the important areas of applications of superhard materials.

Worth mentioning is the ultra-nanocrystalline diamond deposited by plasma-induced chemical vapor deposition (P-CVD) from hydrocarbons strongly diluted by hydrogen (Erdemir et al. 2005; Gruen 1999). This material consists of 3–4 nm size diamond nanocrystals connected by C = C double bonds. Because the deposited films were only few μm thick, reliable data about their load-invariant hardness are not available. Nevertheless the hardness of 1 μm thick coatings has been 100 GPa (see Fig. 4 in Veprek 1999). Besides high hardness, this material has also high corrosion resistance in acidic and basic environment and is biocompatible. Therefore it finds many applications not only as hard coatings on tools from machining of nonferrous materials but also in medicine as protection coatings on implants and the like (Auciello 2010; Auciello and Shi 2010).

2.3 Hardness Enhancement by Ion Bombardment During Thin-Film Deposition

When thin films of ceramic materials are deposited under energetic ion bombardment during the deposition at relatively low homologous temperature of less than about 30% of the melting point, many defects due to displacement damage, formation of vacancies, implantation of interstitial, increase of biaxial compressive stress, and the like are formed. These complex synergistic effects result in an increase of the hardness. For example, Musil et al. (1988) reported hardness of TiN deposited by magnetron sputtering at relatively low temperature of more than 70 GPa (hardness of bulk TiN is about 21 GPa) and that of (TiAlV)N of more than 90 GPa. In another paper, hardness of 47 GPa has been reported for (Ti_{1-x}Al_x)N coatings deposited with the same techniques (Musil and Hruby 2000). These researchers reported also a number of superhard nanocomposites consisting of hard transition nitride and soft, ductile metal that does not form stable nitrides [for a summary, see (Musil 2000)].

There are also papers of other groups reporting enhanced hardness in ceramic coatings deposited under energetic ion bombardment at relatively low homologous temperature which we shall not discuss here because such coatings suffer from two problems: (a) the high biaxial compressive stress that develops as a result of the ion bombardment causing delamination of the coatings from the substrate and (b) the fact that the hardness enhancement is lost when such coatings are annealed to 450–550 °C as illustrated in Fig. 6.5. In that figure, ZrN/Cu, ZrN/Ni, and Cr₂N/Ni are the nanocomposites deposited in the laboratory of Musil and annealed in pure nitrogen in the institute of S.V. (Karvankova et al. 2001). As one can see, upon annealing, the hardness decreases to the usual values of the hardness of the nitrides.

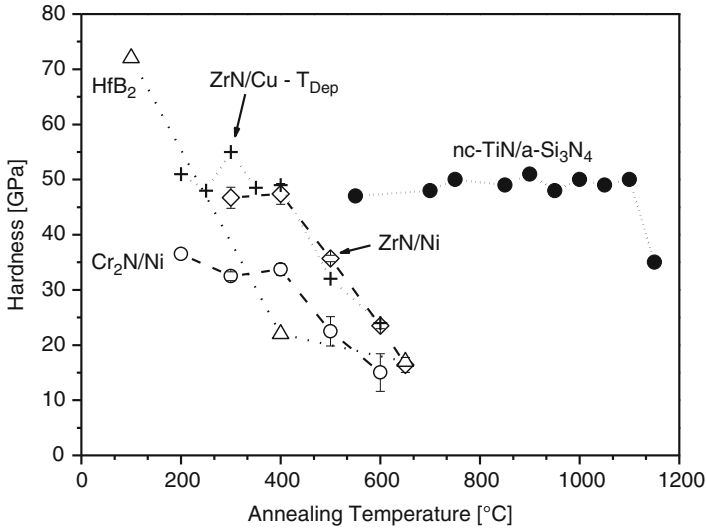


Fig. 6.5 Dependence of the hardness of HfB₂ (Herr and Broszeit 1997), Cr₂N/Ni, and ZrN/Ni (Karvankova et al. 2001) coatings hardened by energetic ion bombardment and stable superhard nc-TiN/a-Si₃N₄ nanocomposites on the temperature of isochronal annealing in pure nitrogen. The hardness was measured at room temperature after each annealing step. The crosses show the dependence of the hardness of the ZrN/Cu coatings on their deposition temperature (Zeman et al. 2000) (From Veprek et al. (2005a) with permission)

Also the HfB₂ coatings deposited by Herr and Broszeit (Herr and Broszeit 1997) lose the hardness enhancement upon annealing.

In contrast, the hardness of the nc-TiN/Si₃N₄ and nc-(Ti_{1-x}Al_x)N/Si₃N₄ nanocomposites formed by spinodal decomposition and deposited without energetic ion bombardment remains stable up to 1100–1200 °C, i.e., of about 65–70 % of the decomposition temperature of Si₃N₄. [For the thermal stability of nc-(Ti_{1-x}Al_x)N/Si₃N₄ nanocomposites up to 1200 °C, see Fig. 2 in Veprek et al. 2004b.] In conventional nanosized or nanostructured materials, the recrystallization and coarsening (Ostwald ripening) occur upon annealing to a homologous temperature of about $T_h = T/T_{\text{Decomp.}} \approx 0.4$. In contrast, the nanocomposites formed by spinodal decomposition with strengthened interfacial Si₃N₄ layer, to be discussed in Sect. 2.5, coarsen only above 1100–1200 °C, and then the hardness, measured after the annealing at room temperature, decreases. This result illustrates the remarkable stabilization of nanostructured material against coarsening. We shall discuss the latter nanocomposites in Sect. 2.5.

These examples show that hardness enhancement by energetic ion bombardment during deposition at relatively low temperature can be achieved in many (probably all) hard ceramic materials. However, the large compressive stress in the coatings and loss of the hardness enhancement upon annealing to relatively modest temperatures are severe obstacles for their application.

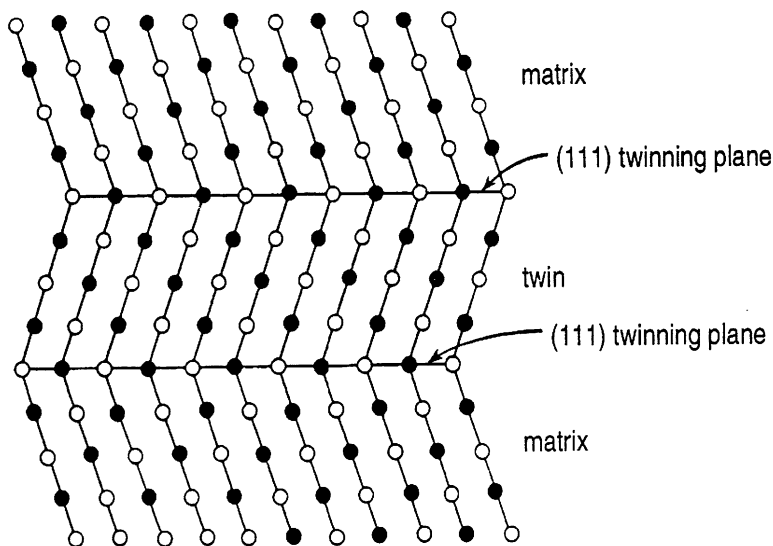


Fig. 6.6 Example of a twin and twinning boundary in an fcc lattice (Reproduced from Gottstein (2004) with permission)

2.4 Hardness Enhancement by Low-Energy Interfaces

Stacking faults and twins are low-energy, coherent grain boundaries (Gottstein 2004), whose “destabilizing” energy is less than about 10% of the energy of common large-angle grain boundaries. Because the low-energy grain boundaries are only one monolayer thin (see Fig. 6.6), whereas the large-angle grain boundaries are 3–4 crystal planes thick, the fraction of the atoms within the low-energy grain boundaries is—for a given grain size—much smaller. Thus, one expects that the “strongest size” should be shifted to smaller crystallite size as compared to the case of common large-angle grain boundaries. With reference to Fig. 6.1, one logically expects that the strengthening due to smaller crystallite size should continue to increase following the “Hall-Petch” curve with crystallite size decreasing down to a few nm small nanocrystals, because the weakening due to grain-boundary shear will be much less (Huang et al. 2014; Tian et al. 2013; Xu and Tian 2015). Therefore, one expects large strengthening and hardening in nanosized materials with low-energy grain boundaries. Indeed, Mg alloys with a large density of stacking faults achieved the highest strength ever reported in these materials (Jian et al. 2013). The high density of the stacking faults has been achieved by severe plastic deformation of Mg alloy sheets upon a repeated rolling. Although these strong Mg alloys are not superhard, we mention them here to underline the general nature of this strengthening mechanism.

The recently synthesized nanotwinned c-BN (Tian et al. 2013) and diamond (Huang et al. 2014; Xu and Tian 2015) provide an important support to this

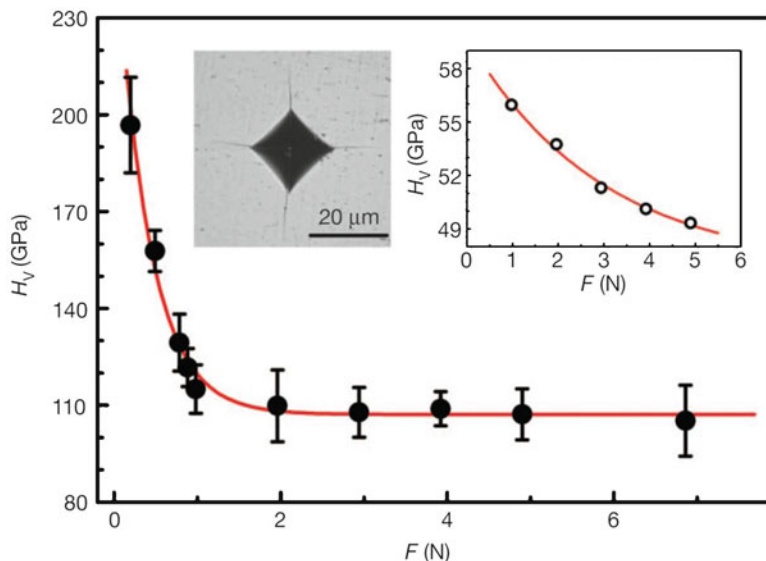


Fig. 6.7 Vickers hardness of nanotwinned c-BN vs. applied load and SE micrograph of an indent at a large load of 19.6 N. The inset on the right shows the hardness of bulk c-BN vs. applied load (From Tian et al. (2013) with permission)

hypothesis. In the nt-c-BN, the average distance between the twins was about 3.8 nm, and the hardness reached load-invariant value of 108 GPa at a load of ≥ 1.5 N. The material has been prepared by HTHP treatment of a special turbostratic onion-like BN nanoparticle precursor material. The usual HTHP synthesis of c-BN from the hexagonal “graphite-like” boron nitride yields nanocrystalline material with grain size ≥ 10 nm (Sumiya et al. 2000; Dub and Petrusha 2006; Dubrovinskaia et al. 2007; Solozhenko et al. 2012). These nanograins c-BN and c- and w-BN nanocomposites reach hardness of “only” ≤ 85 GPa because they have large-angle grain boundaries.

Figure 6.7 shows the Vickers hardness of nt-c-BN vs. the applied load and a scanning electron micrograph (SEM) image of an indent at a large load of 19.6 N. Obviously, the load-invariant hardness is reached already at a relatively low load of 1–1.5 N, whereas for bulk c-BN, the hardness continues to decrease even at a load of 5 N (see inset on the upper right-hand side of Fig. 6.7). The nanotwinned c-BN has also high toughness of $\geq 12 \text{ MPa} \cdot \text{m}^{0.5}$ which is much higher than that of bulk c-BN of about $2.8 \text{ MPa} \cdot \text{m}^{0.5}$ and higher oxidation resistance than c-BN. We refer to the paper of Tian et al. for further details.

The ultrahard nanotwinned diamond has been prepared from onion-like carbon by HTHP synthesis in a similar way as the nt-c-BN (Huang et al. 2014). Figure 6.8a shows the distribution of the twin thickness measured by high-resolution transmission electron microscopy (HRTEM), and Fig. 6.8b shows the hardness vs. the applied load. The average thickness of the twins of 5 nm is close to that of nt-c-BN, but the load-invariant hardness of about 200 GPa is much higher than that of nt-c-BN and of natural diamond.

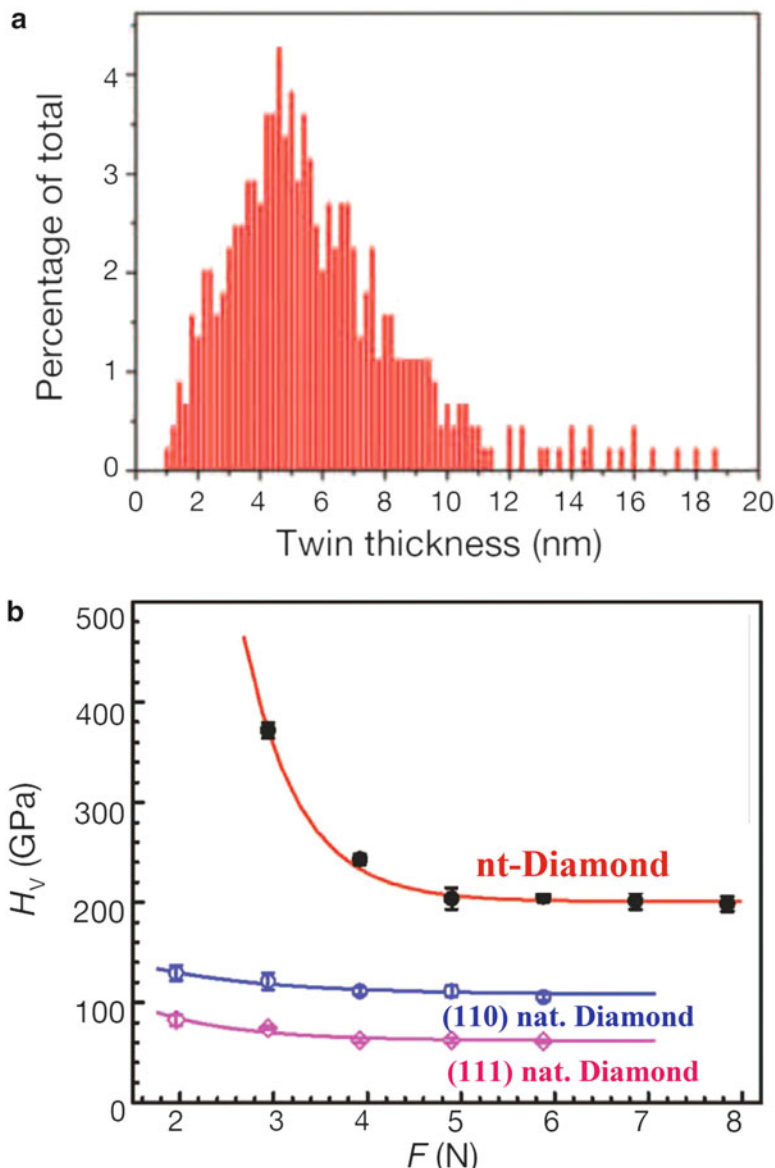


Fig. 6.8 (a) Distribution of the thickness of the nanotwins measured by HRTEM yielding an average value of about 5 nm, (b) Vickers hardness of nt-diamond (red), (110) (blue), and (111) face of natural diamond vs. applied load (From Huang et al. (2014) with permission)

A critical reader will ask how it is possible to measure such a high hardness using diamond indenter with a lower hardness of 70–100 GPa. This is indeed possible because the indenter is loaded mainly in compression, whereas the material being indented is loaded in shear, as shown by the slip-line field theory (Hill 1950) and

illustrated in Fig. 13.8 in McClintock and Argon (1966) to which we refer for further details. Figure 29 in Veprek (2013) shows that the materials flow in the diamond indenter under the load and within the contact with the material being indented occurs directed into the indenter, as expected under a pressure loading. Diamond, like other materials with cubic structure, sustains up to eight times larger load in compression than in shear (Eremets et al. 2005; Field 1992). We emphasize this point here, because the work of Tian and Huang has been criticized in a harsh manner using incompetent arguments that “one cannot measure hardness higher than diamond using diamond indenter” (Saxonian 2015).

We believe that these three examples strongly support the concept for the design of extrinsically superhard, nanostructured material with low-energy grain boundaries. As shown by the example of the Mg alloy, this concept is not limited to superhard materials only, but it applies generally for the design of strong and tough materials. The disadvantage of the HTHP synthesis is so far the small size of the samples which can be prepared. The Mg alloys with the nanosized stacking faults have been prepared by severe plastic deformation using repeated rolling, which is a technique applied on industrial scale to produce large metal sheets. Nevertheless, there is some hope that the HTHP techniques for the synthesis of nt-c-BN and nt-diamond can be further developed and scaled for industrial production.

2.5 Superhard Nanocomposites with Strengthened Interfacial Layer

In this section, we shall discuss the superhard nanocomposites consisting of nanocrystals of certain transition metal nitrides embedded in a thin interfacial layer of silicon nitride. These materials can reach a very high hardness of more than 100 GPa when correctly prepared and sufficiently free of impurities, mainly oxygen. They are produced by plasma chemical or physical vapor deposition (P-CVD or PVD) as thin films and can be applied as wear-protection coatings on tools for machining, forming, stamping, injection molding, and the like. The Czech company SHM has pioneered the industrialization of these coatings since 1996 when tools for machining coated with the nc-(Ti_{1-x}Al_x)N/Si₃N₄ nanocomposites were offered on the market for the first time. We shall discuss the generic concept for their design, the properties of the nanocomposites, and their limitations as regards the choice of the system and purity. It will be shown that not all systems meet the conditions needed to reach superhardness, and those which do meet them can reach high hardness only when carefully prepared and free of impurities. We shall start with the nc-TiN/Si₃N₄ nanocomposites because majority of the information is available for this system. Afterward, we shall discuss which of the other TmN/Si₃N₄ and TmN/XY systems (Tm, transition metal; XY another covalent compound instead of Si₃N₄) can meet the requirements to be superhard, and we shall finish with a brief summary of the industrial application.

A short remark: Attempts to prepare the nc-TiN/Si₃N₄ nanocomposites as bulk ceramics by means of high-temperature high-pressure sintering have brought only limited yet important improvement in the hardness and fracture toughness to 25 GPa and 6 MPa · m^{0.5}, respectively. In this case, the grain size varied between 33 and 340 nm (Bläß et al. 2015).

2.5.1 Superhard nc-TiN/Si₃N₄ Nanocomposites as a Model System

The Role of the Interfaces

Figure 6.9a shows the hardness enhancement of nc-TiN/Si₃N₄, nc-W₂N/Si₃N₄, and nc-VN/Si₃N₄ superhard nanocomposites as function of the Si content (Veprek and Veprek-Heijman 2007), and Fig. 6.9b shows the dependence of the lattice dilatation of nanocrystalline silicon (nc-Si) and of the TiN nanocrystals in nc-TiN/Si₃N₄ superhard nanocomposites as function of the crystallite size. In Fig. 6.9b, the values for nc-Si have been extracted from Veprek et al. (1982), whereas those for the nc-TiN/Si₃N₄ nanocomposites were taken from Veprek and Reiprich (1995). The crystallite size of nc-Si has been controlled by the deposition temperature between about 80 °C and 300 °C. In the case of the nanocomposites, the deposition temperature has been kept constant at 550 °C, and the size of the TiN nanocrystals was dependent on the content of Si₃N₄ as seen in Fig. 6.9a.

The hardness enhancement by a factor of up to 3.6 is achieved when the thickness of the Si₃N₄ interfacial layer is about one monolayer (1 ML) at Si content of about 7 % in all three nanocomposites, but this enhancement is lost when the thickness reaches 2 ML, i.e., Si content of about 14 % (Fig. 6.9a). At the maximum hardness, the crystallite size decreases to about 3 nm, and upon further increase of the Si₃N₄ layer thickness, the crystallite size increases again. This increase has been found only when the nanocomposites were deposited by P-CVD in high-frequency glow discharge where the bombardment of the growing film by energetic ions was negligible (Veprek and Reiprich 1995). When the deposition has been done under condition of energetic ion bombardment, the crystallite size decreased with increasing Si₃N₄ content in a similar manner to about 3 nm but remained constant upon a further increase of Si₃N₄ because of the effect of ion bombardment. The strain seen in Fig. 6.9b increases with increasing Si₃N₄ content up to the maximum hardness and minimum crystallite size and decreases again upon a further increase of the Si₃N₄ content [see Fig. 3 in Veprek et al. (2000)].

In order to understand this behavior, we have to briefly discuss the nc-Si first (Veprek et al. 1982). There is a density deficit within the grain boundaries of polycrystalline materials which imposes a tensile strain on the Si nanocrystals. For a crystallite size of < 10 nm, this appears as dilatation of the lattice parameter of the Si nanocrystals that has been measured by X-ray diffraction (XRD). This dilatation increases with decreasing crystallite size because there are less Si atoms balancing the stress from the grain boundaries by elastic elongation of the Si-Si bonds. Therefore, also the elastic strain energy increases. When, at the

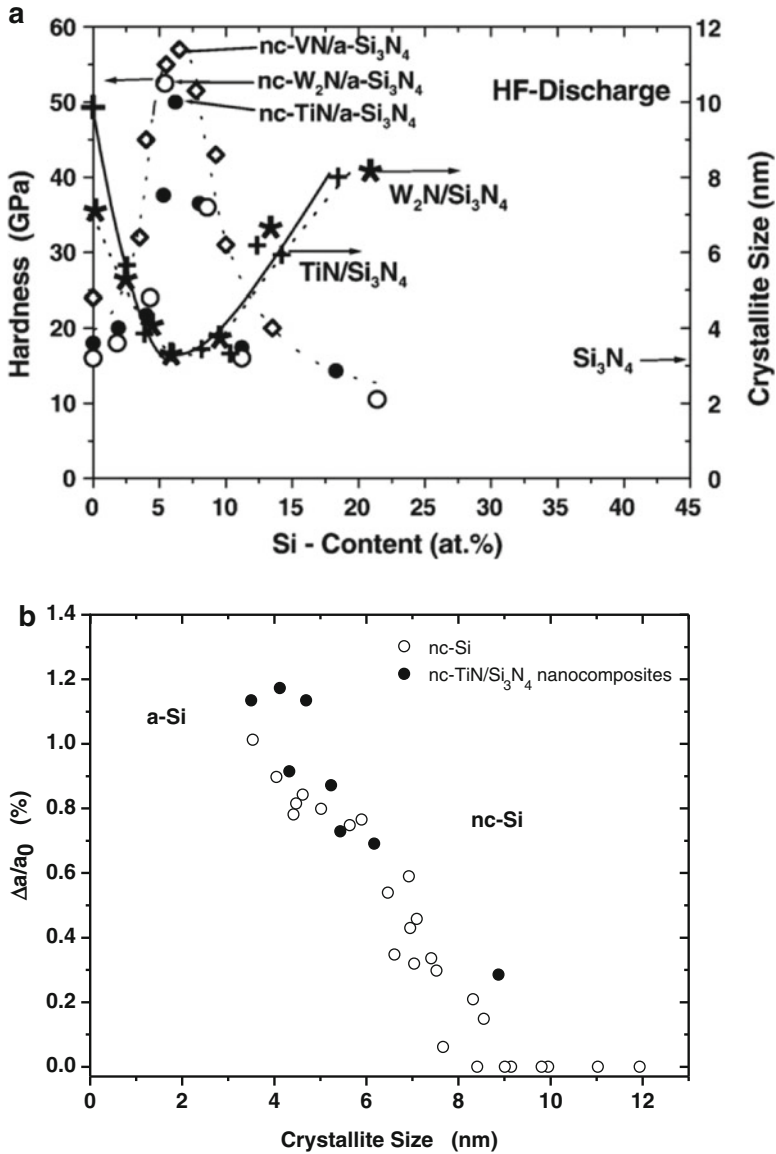


Fig. 6.9 (a) Hardness and crystallite size as function of silicon content for three nc-TmN/Si₃N₄ nanocomposites. Notice that all silicon was present as Si₃N₄, not dissolved in TiN (from Veprek and Veprek-Heijman (2007) with permission) and (b) lattice dilatation due to the tensile strain within the grain boundaries for nanocrystalline silicon nc-Si and superhard nc-TiN/Si₃N₄ nanocomposites

crystallite size of about 3.5 nm, the strain reaches $\geq 1\%$ (corresponding to a “negative pressure” of about 10 GPa), the elastic strain energy is equal to the excess energy of amorphous silicon (a-Si), i.e., nc-Si is unstable with respect to a-Si for a smaller crystallite size (for further details, see Veprek et al. 1982).

The situation is more complex in the nanocomposites because of several reasons: The lattice misfit between TiN and Si_3N_4 contributes to the measured lattice dilatation which reaches 1.2% for the smallest crystallite size of about 3 nm. However, with a further increase of the silicon nitride content, the lattice dilatation of the TiN nanocrystals decreases because the thicker Si_3N_4 interfacial layer, which is weaker than the TiN, compensates the strain [see Fig. 5 in Veprek and Reiprich (1995)]. This explains why there is a minimum crystallite size of about 3 nm in the nanocomposites and why the TiN remains crystalline. It should be mentioned that due to the measured strain, there is a large random stress in the nanocomposites reaching a value of about 7–10 GPa for the smallest crystallite size [see Fig. 5 in Niederhofer et al. (1999)].

Strengthening of the Interfacial Si_3N_4 Layer. The question arises as to why the system chooses minimum crystallite size when the hardness reaches a maximum? The grain boundaries have excess energy and, therefore, destabilize any polycrystalline system. This is the general reason for recrystallization and coarsening of small-grain polycrystals upon annealing (“Ostwald ripening”). The only logical explanation of the behavior observed in the three nc-TmN/ Si_3N_4 systems (Fig. 6.9a) was that the nc-TmN/1 ML- Si_3N_4 /nc-TmN interface is somewhat stabilized as compared to conventional large-angle grain boundaries in polycrystalline TmN. This suggestion caused for many years controversial discussions with the specialists, until first-principle density functional theory (DFT) calculations confirmed it. We shall briefly summarize the understanding of the nc-TiN/ Si_3N_4 nanocomposites that has been achieved so far.

Hao et al. conducted the first DFT investigations into the nc-TiN/ Si_3N_4 nanocomposites (Hao et al. 2006a, b). These researchers have shown that the tensile strength of the 1 ML Si_3N_4 -like¹ interfacial layer is larger than that of an ideal Si_3N_4 single crystal. More detailed DFT studies of this system by Zhang et al. have shown that the SiN_x interfacial layer is strengthened by valence charge transfer from the TiN nanocrystals (Zhang et al. 2009a, b). The valence charge transfer is a consequence of the fact that the electronegativity of Si (1.8) is larger than that of Ti (1.5). To illustrate this strengthening, we reproduce in Fig. 6.10 the valence charge density difference (VCDD) of the TiN(111)/1 ML-SiN/TiN(111) interface.

¹The stoichiometry of 1 ML thick interfacial layer between TiN slabs deviates from that of the Si_3N_4 depending on the (hkl) nature of the interface. We write Si_3N_4 -like because the X-ray photoelectron spectroscopic (XPS) studies have shown that silicon is fourfold coordinated to nitrogen like in Si_3N_4 crystal.

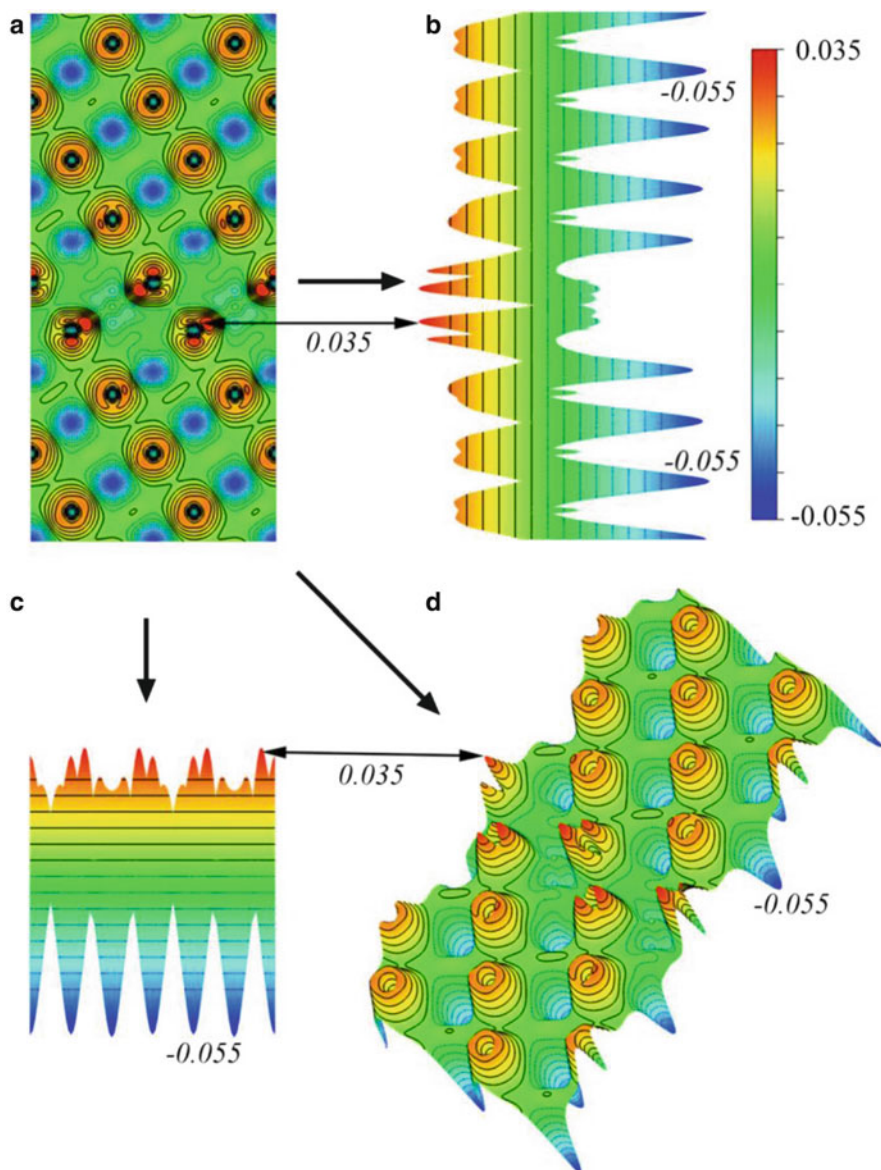


Fig. 6.10 (Color online) (a) Valence charge density difference of the TiN(111)/1 ML-SiN/TiN (111) interface and the corresponding bird's eye view profile seen from different directions marked by arrows: (b) left view and (c) top view and (d) side view. The color scale runs from -0.055 at bottom blue to 0.035 electrons/Bohr³ at top red. The small (black) italic numbers indicate the values of the valence charge density difference (From Zhang et al. (2009b) with permission)

Because the VCDD on nitrogen within the SiN layer is higher than that on nitrogen in the TiN and also the VCDD on Si is higher than the VCDD on Ti, it is clear that the 1 ML SiN interfacial layer is strengthened in agreement with the calculations of Hao et al. However, this does not mean that the whole TiN/1 ML-SiN/TiN interface is stronger than the ideal TiN single crystal. As a consequence of the valence charge transfer, the Ti-N bonds in the TiN nanocrystals close to the Si₃N₄ interface are weakened and thus represent the weak links in the system where, upon a tensile or shear load, the decohesion or shear occurs. For further details, we refer to the quoted papers (Zhang et al. 2009a, b).

Here we shall only explain the experimental observation seen in Fig. 6.9a that the hardness enhancement is lost when the Si₃N₄-like interfacial layer is 2 ML thick. In the case of 2 ML thick interfacial Si₃N₄ layer, the weakening of the Ti-N bonds due to the valence charge transfer to the 2 ML interfacial layer is too large and the whole system loses its strength enhancement. Upon a tensile load, the decohesion occurs at the interface between the SiN (or Si₃N₄) and TiN [for further details, see Zhang et al. (2010b); Ivashchenko et al. (2015)]. To summarize, because TiN is much stronger than Si₃N₄, the nanocomposites gain hardness when the interfacial Si₃N₄-like layer is one monolayer thin, but this enhancement is lost when the thickness is two monolayers or more, because too much valence charge density is transferred from TiN to the ≥ 2 ML SiN_x.

The limitation of the DFT is that it assumes a system with the atoms at rest, which means that the calculations are limited to 0 K. Therefore, Ivashchenko et al. conducted comparative studies by means of first-principle quantum molecular dynamics (QMD) that allows for thermal motions of the atoms (phonons) and conducts the DFT calculations in small time steps of this motion. Such calculations are very much computing time-consuming. Nevertheless, the calculations performed so far confirmed all essential results obtained in the earlier DFT studies by Zhang et al. which have been done for pseudomorphologically stabilized fcc-SiN that is unstable as bulk crystal. Ivashchenko et al. included in their calculations also Si₃N₄-like interfacial layers.

Interestingly, these researchers have found that the fcc-(111)-1 ML-SiN interfacial layer is stable also at very high temperatures although, according to the ordinary thermodynamics at macroscale, it should decompose according to the reaction $4\text{SiN} \rightarrow \text{Si}_3\text{N}_4 + \text{Si}$. This stability at nanoscale is probably due to the fact that for the decomposition reaction to occur, several atoms have to move simultaneously, i.e., the reaction requires a minimum volume for the “nucleation,” which is difficult to occur in 1 ML layer. This example shows that also interfaces, which are unstable at macroscale, should not be ruled out at nanoscale. We still know very little about the nature of the interfaces in the nanocomposites. We refer to the relevant papers of Ivashchenko et al. for further details (Ivashchenko et al. 2012, 2015).

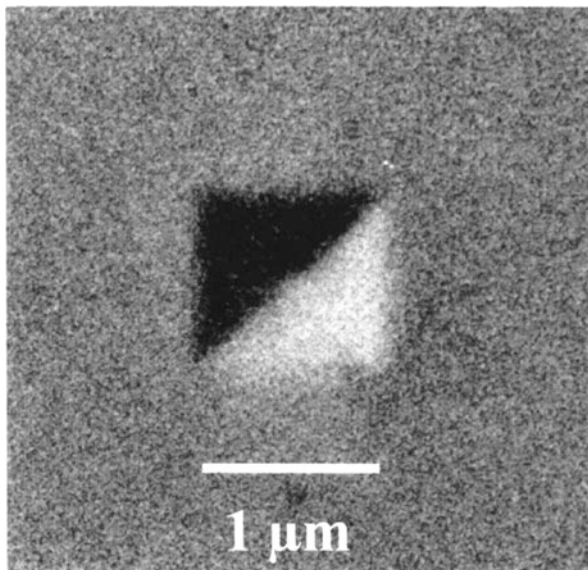
The Theoretically Achievable Hardness of the nc-TiN/Si₃N₄ Nanocomposites

The DFT and QMD studies enabled to calculate the shear resistance of the interfaces for a variety of (hkl) interfaces. These are of course lower than the ideal shear strengths of TiN single crystal. However, one has to remember that under the conditions of fully developed plasticity, where the correct, load-invariant hardness is measured, there is no ideal crystal but many defects, such as dislocations, grain boundaries, and in some cases metastable or unstable phases with much lower shear resistance as discussed above. Therefore, the values of shear resistance of a variety of (hkl) interfaces between about 11.5 and 22 GPa calculated by DFT (Veprek et al. 2007) and about 15–32 GPa calculated by QMD (Ivashchenko et al. 2015) can be used as shear resistances of the interfaces in the nanocomposites where the plastic flow occurs. We refer to these papers for further detail of the calculations. Here we only state that these calculations yielded an achievable hardness of the nanocomposites of 130–170 GPa, significantly above the hardness of natural diamond.

Therefore the experimental results published earlier by Veprek's group on the hardness of the nc-TiN/Si₃N₄ nanocomposites up to 70 GPa (see Fig. 6.11) and for the quasi-ternary nc-TiN/Si₃N₄/TiSi₂ nanocomposites above 100 GPa [see Fig. 5b in Veprek and Veprek-Heijman (2012) and Fig. 4.6b in Chap. 4 of this book] can be understood also from the theoretical point of view: There is no dislocation activity in 3 nm small nanocrystals whose strengths approach the ideal strength of a perfect single crystal. The high-pressure XRD studies of Prilliman et al. have shown that the TiN nanocrystals deform only elastically and the grain boundaries are the carrier of the plastic flow (Prilliman et al. 2006). Therefore, the plastic resistance of the grain boundaries determines the strength and hardness of the nanocomposites. And because the interfaces in the nc-TiN/Si₃N₄ nanocomposites are strengthened by the valence charge transfer, their plastic flow resistance is significantly higher than that of ordinary large-angle grain boundaries in highly deformed polycrystalline TiN.

Of course, there are still many open questions. The DFT and QMD calculations have been done for selected (hkl) interfaces in the TiN/Si_xN_y/TiN heterostructures, whereas the nanocomposites consist of an unknown variety of (hkl) interface which are only 1–2 nm small. Moreover, there are many boundaries between these small interfaces and also triple junctions whose role is difficult to estimate (see, e.g., Zhao et al. 2011, 2012). Therefore, it is difficult to know what exactly is happening in these nanosized grain boundaries upon a load. Nevertheless, the DFT and QMD calculations provide a solid basis for the understanding of the very high hardness in the nanocomposites.

Fig. 6.11 SE micrograph of an indentation into 8 μm thick nc-TiN/a-Si₃N₄ nanocomposite coating with a Vickers diamond indenter at a load of 110 mN (From Veprek and Veprek-Heijman (2012) with permission)



The Mechanism of the Formation of the Nanocomposites

When the nc-TiN/Si₃N₄ (and related) nanocomposites are deposited by PVD or P-CVD, the individual atoms are arriving at the surface of the growing film randomly, i.e., a homogeneous solid Ti_x-Si_y-N_z solution is formed with composition given by the deposition parameters used. This solid solution has to decompose forming the nc-TiN/Si₃N₄ nanocomposite. In this system, the decomposition occurs by spinodal mechanism.² Figure 6.12 shows the Gibbs free energy for the Ti_x-Si_y-N_z system calculated by means of a semiempirical thermodynamics formula based on the sub-lattice model for different activities of nitrogen (Zhang and Veprek 2006). In later work, a combined DFT calculation and thermodynamical modeling have been used and very similar results have been obtained (Zhang and Veprek 2008). As one can see in Fig. 6.12, the system is chemically spinodal within the whole range of the composition even at the lowest nitrogen pressure used during PVD. At the composition corresponding to the 1 ML of interfacial Si₃N₄ (i.e., the maximum hardness), the de-mixing energy is more than 300 kJ/mol, about two orders of magnitude larger than in typical metallic alloys. This is a very high de-mixing energy. Therefore, the system is spinodal even if there is a certain lattice

²The term “spinodal” has been introduced by Van der Waals as a footnote in his Ph.D thesis, without any particular linguistic meaning, to assign the part of his isotherm between the binodal points where the second derivative is negative. Spinodal decompositions of a solid solution (or, e.g., copolymers) occur when the second derivative of the Gibbs free energy of that solution is negative, i.e., the system is inherently thermodynamically unstable [see Zhang and Veprek (2006) and references therein].

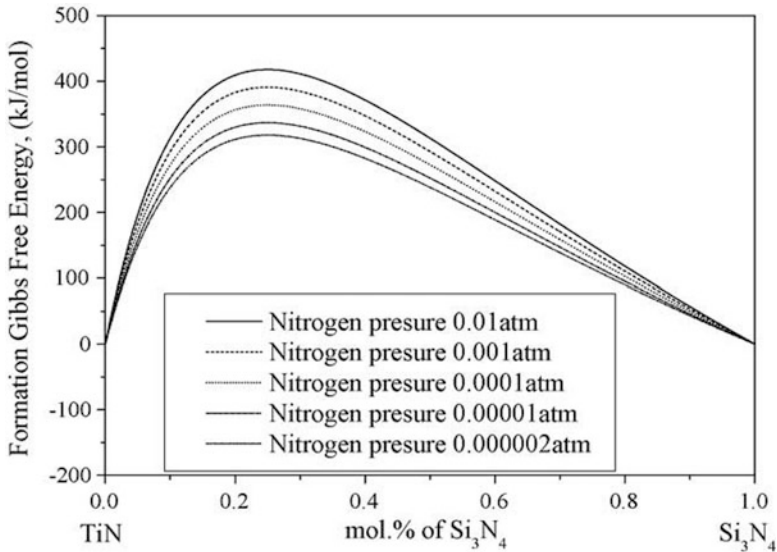


Fig. 6.12 Gibbs free energy of the formation of mixed TiN+ Si_3N_4 system at temperature of 873 K (corresponding to the *upper* limit of the deposition temperature used) for five different pressures of nitrogen used in the experimental work. TiN and Si_3N_4 have been taken as the reference phases (From Zhang and Veprek (2006) with permission)

mismatch between the TiN and Si_3N_4 -like interfacial layer [for the details of the calculation, see Zhang and Veprek (2006)]. Because the spinodal decomposition yields a nanostructure with well-defined periodicity (Schmalzried 1995; Porter and Easterling 2001), there is a narrow size distribution of the TiN nanocrystals, as observed experimentally by means of HRTEM (Christiansen et al. 1998).

It should be emphasized that Christiansen et al. studied several nc-TiN/ Si_3N_4 samples with different Si_3N_4 content up to 15 at.% of Si where the hardness enhancement is already lost (c.f. Fig. 6.9a). For each sample, several tens of HRTEM micrographs have been done and investigated. The nanostructures seen in the HRTEM micrographs were the same in plain as well as in cross-sectional view, and there was no indication of any columnar morphology, in contrast to many later reports of other groups (see later). The TiN nanocrystals were randomly oriented and of fairly regular shape with a narrow size distribution. (The random distribution of the TiN nanocrystals has also been confirmed by XRD [see Fig. 3 in Niederhofer et al. (1999)].) All the several hundred TiN nanocrystals investigated were without any defects, such as dissolved Si or oxygen. This is in agreement with the XPS studies mentioned above and with the fact that stoichiometric and pure transition metal nitrides and Si_3N_4 are immiscible (Rogl and Schuster 1992). As we shall show later, the “miscibility of Si in TiN” and columnar morphology reported in some later papers is due to oxygen impurities or other defects.

Conditions Needed to Assure that the Spinodal Decomposition Will Occur During the Deposition. The nitrogen activity (partial pressure) during the deposition is the thermodynamic driving force for the decomposition of an unstable Tm-Si-N solid solution. The rate of the decomposition is kinetically controlled by diffusion. Therefore, both the nitrogen pressure and the deposition temperature must be sufficiently high to assure that the spinodal decomposition and formation of stable nanostructure are completed during the deposition. Moreover, because the maximum hardness is achieved when the interfacial Si_3N_4 layer is about 1 ML thick, the Tm-Si-N system must be spinodal with a high de-mixing energy, because only in such a case the interfaces can be sharp (Veprek and Reiprich 1995). Figure 6.12 shows that even at the relatively low nitrogen pressure used in PVD, the Ti-Si-N system is spinodal. It has been found experimentally (Veprek and Reiprich 1995), and later on calculated from the known diffusion coefficients (Veprek et al. 2006), that a deposition temperature of ≥ 550 °C is needed to assure that the nanostructure will form during the deposition.

When these conditions are met, superhard nc-TiN/ Si_3N_4 nanocomposites with hardness of about 70 GPa can be prepared as shown in Fig. 6.11 (Veprek and Veprek-Heijman 2012). The scanning electron micrograph (SEM) shows an indentation into 8 μm thick nc-TiN/ Si_3N_4 nanocomposite coating with a Vickers diamond indenter at a load of 110 mN. One notices that a plastically deformed indentation area of 1 μm^2 ($=10^{-12}$ m^2) produced under a load of 100 mN corresponds to a Meyer hardness of 0.1 $\text{N}/10^{-12}$ $\text{m}^2 = 10^{11}$ $\text{N}/\text{m}^2 = 100$ GPa.³ For a Vickers indenter of an ideal shape, the Meyer and Vickers hardness is related to as $H_{\text{Vickers}} = 0.927 H_{\text{Meyer's}}$ (Tabor 1951). But because the diamond indenter deforms plastically upon indentation into superhard materials until the tip becomes dull with a radius of 0.5–0.7 μm (Veprek-Heijman et al. 2009), the Vickers and Meyer hardness is for a relatively small indentation shown in Fig. 6.11 almost identical.

In order to achieve such a high and long-term stable hardness, one must meet the conditions outlined above and the oxygen impurities must not exceed 100–200 ppm. Hardness in excess of 100 GPa has been obtained in the quasi-ternary nc-TiN/ Si_3N_4 /TiSi₂ nanocomposites [see Fig. 4.6 in Chap. 4 of this book and also Fig. 5 in Veprek and Veprek-Heijman (2012)] because the TiSi₂ is efficiently trapping the minor oxygen impurities. However, these nanocomposites lose the high hardness after 4–6 months because of degradation of the TiSi₂ as shown already in Veprek et al. (2005a) and discussed in some details recently (Veprek 2013). We refer to these papers for further details.

In conclusion to this section, long-term stable quasi-binary nc-TiN/ Si_3N_4 nanocomposites with hardness of about 70 GPa have been prepared when the oxygen impurities were very low of about 100 ppm. Furthermore, many nc-TmN/

³ Meyer's and Vickers hardness is the applied load divided by the projected and total contact area of the indent, respectively.

Si_3N_4 coatings with hardness ≥ 50 GPa have been prepared when the oxygen impurities did not exceed several 100 ppm (Veprek et al. 2000; Veprek and Veprek-Heijman 2012; Veprek 2013). We refer to these papers for further detail. On the basis of several papers published by other groups, it has been shown that when these conditions are not fulfilled, superhard nanocomposites cannot be obtained (Veprek et al. 2006). This will be the subject of the next session.

Impurities and Inappropriate Deposition Conditions Are Limiting the Achievable Hardness of the Nanocomposites

The failure of several groups to obtain the high hardness in the nc-TiN/ Si_3N_4 nanocomposites has been either due to inappropriate deposition conditions used (mainly a too low temperature) or oxygen impurities as already discussed several years ago (Veprek et al. 2006; Veprek and Veprek-Heijman 2012). This is illustrated in Fig. 6.13 that shows the maximum achievable hardness in the nc-TiN/ Si_3N_4 nanocomposite coatings as a function of oxygen impurities (Veprek et al. 2005b). It should be noted that there are results from five different P-CVD and PVD apparatuses from three different countries. Since writing that paper more than 10 years ago, many more results could be added in the range of oxygen impurity of $> 0.5\%$ and hardness below 40 GPa, but we believe that the data in Fig. 6.13 are

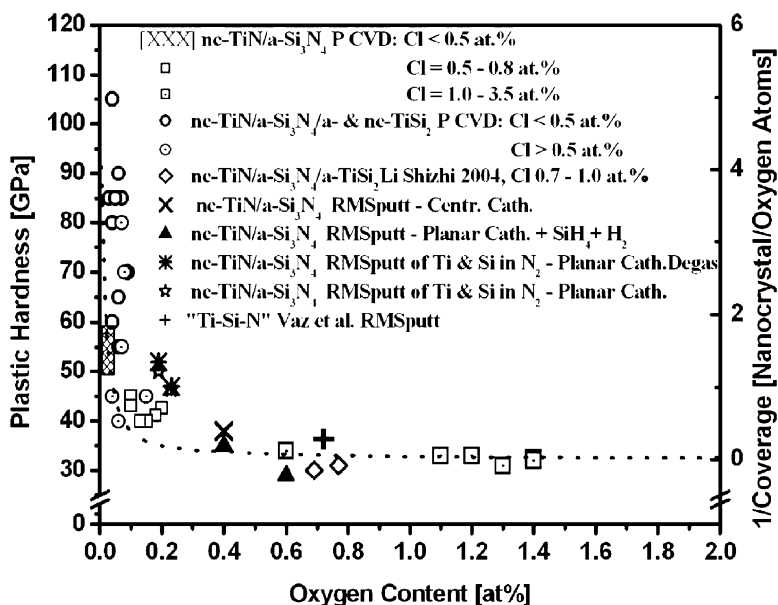


Fig. 6.13 Maximum achievable hardness in the nc-TiN/ Si_3N_4 nanocomposite coatings vs. oxygen impurities. Note that there are results from five different P-CVD and PVD apparatuses from three different countries (From Veprek et al. (2005b) with permission)

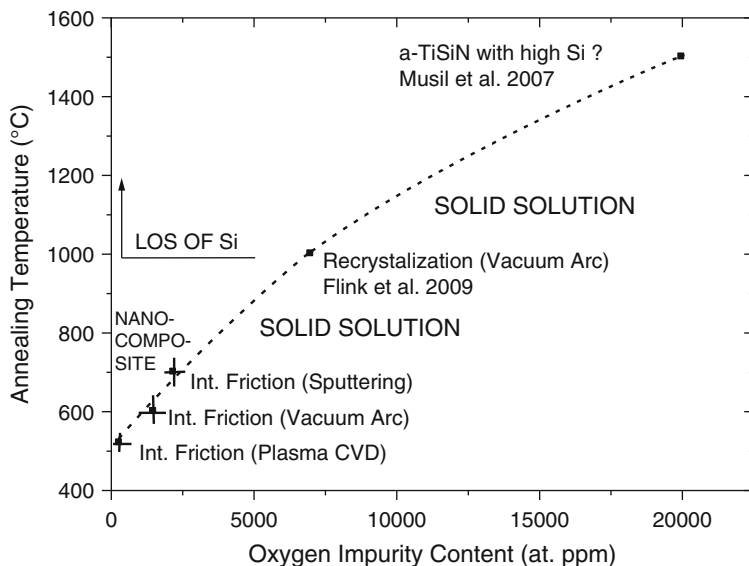


Fig. 6.14 Temperature needed for the decomposition of the Ti-Si-N solid solution and the formation of stable nc-TiN/Si₃N₄ nanostructure (the three points denoted “Int. Friction” on the left), the recrystallization of the solid solution, and the stability limit of Ti-Si-N coatings with high Si content (From Veprek and Veprek-Heijman (2012) with permission)

sufficient to show the critical role of oxygen impurities. The high hardness of > 40–50 GPa can be achieved only when the oxygen impurity content is of few 100 ppm. The reason is that the Si-O bond is the strongest one within the whole Ti-Si-N (and other Tm-Si-N) system. Therefore, oxygen forms $\equiv \text{Si-O-Si} \equiv$ clusters which degrade the interfacial Si₃N₄ layer [see Fig. 2 in Veprek et al. (2005b)] and hinder the diffusion and formation of the nanostructure as we shall discuss now. Other impurities, such as hydrogen and carbon, also degrade the mechanical properties of the nanocomposites (Veprek et al. 2004a), but oxygen is the most “dangerous” impurity because of its high electronegativity and strong Si-O bond.

The temperature needed for the decomposition of the solid solution and formation of the stable nanostructure increases with increasing impurity oxygen content, as shown in Fig. 6.14. The two points denoted “Int. Friction (Plasma CVD)” and “Int. Friction (Sputtering)” on the left lower part correspond to the formation of superhard nc-TiN/Si₃N₄ nanocomposites by P-CVD and reactive magnetron sputtering in the institute of S.V., whereas the point denoted “Int. Friction (Vacuum Arc)” corresponds to nc-(Ti_{1-x}Al_x)N/Si₃N₄ nanocomposites deposited by vacuum arc in an industrial coating system of the SHM company (SHM). The point “recrystallization (vacuum arc)” corresponds to the “recrystallization” of the Ti-Si-N solid solution “stable” up to this point as reported by Flink et al. (2009), and the point “a-TiSiN with high Si” describes the stability limit of Ti-Si-N coatings with high Si content (Musil et al. 2007).

Flink et al. reported already in 2005 (Flink et al. 2005) about the high stability of the Ti-Si-N solid solution, but in that paper, the concentration of oxygen impurities has not been given. In a later paper, they confirmed the high stability of the solid solution up to 1000 °C and reported also the oxygen impurity content of about 0.7–0.8 % (7000–8000 ppm) for coatings with Si content of 7–9 % where the maximum hardness should be found. However, it is not possible to prepare superhard nanocomposites under such conditions because, as well known from silicon technology, silicon is lost by evaporation of SiO that is volatile above 900 °C. Indeed, using atom probe tomography, Tang et al. did not find any Si₃N₄-like interfacial layer in Ti-Si-N coatings with oxygen impurity content of about 1.2–1.4 at.% (Tang et al. 2010). According to the results shown in Fig. 6.14, the samples used by these researchers would have to be annealed at a high temperature of about 1200 °C to reach the “recrystallization.” Flink et al. also reported very high density of dislocations of about $1 \cdot 10^{14} \text{ cm}^{-2}$ in their Ti-Si-N films and stated that this “corresponds to values found for heavily cold work-hardened material” (Flink et al. 2009). Critical reader will realize that this value is the order of magnitude too high for cold work-hardened material (Argon 2008),⁴ but it can be explained by the oxygen impurities: Taking the reported concentration of about 0.8 at.% and assuming that the thickness of the samples used for the TEM study was about 20–30 nm yield the areal density of the O-related defects of about 0.6 to $1 \times 10^{14} \text{ cm}^{-2}$.

When, in a later work, the oxygen impurity has been decreased below the detection limit of 0.1 % (1000 ppm) of the analytic techniques used by this group, the homogeneous solid solution could be grown at 550 °C epitaxially on TiN up to a critical thickness of few tens of nm. The segregation of Si to the grain boundaries was seen for thicker layers, but it seems to be still incomplete (Eriksson et al. 2014). It remains an open question if the TiN and Si₃N₄ phases would segregate completely in these experiments when the oxygen impurity content would be only few 100 ppm. According to our results and those available in the literature (Rogl and Schuster 1992), the segregation will be completed if the impurity content will be sufficiently low.

There is a fundamental question regarding the nanostructure formation in the Ti-Si-N coatings deposited by PVD because all papers known to us reported columnar morphology. In our own studies using reactive magnetron sputtering, we have also observed dense morphology which appeared isotropic in the SEM [see Fig. 14 in Prochazka et al. (2004)], but columnar, although very dense morphology could be seen in HRTEM. However, the oxygen impurity of about 1000–1500 ppm was also much larger in our coatings deposited by reactive sputtering than in the nc-TiN/

⁴ At a dislocation concentration of 10^{14} cm^{-2} , the long-range order is lost (Ninomiya 1978) and amorphization occurs (Nastasi et al. 1996). High dislocation density of 10^{14} cm^{-2} can be formed by a powerful 10 ps laser pulse, but the dislocation density quickly decays to 10^{13} cm^{-2} after only 140 ps (Bringa et al. 2006).

Si_3N_4 nanocomposites deposited by P-CVD, which had fully isotropic nature (see above). Nevertheless, the segregation of the TiN and Si_3N_4 has been clearly seen also in our coatings deposited by sputtering [see Fig. 9 in Veprek (2013)]. This question will remain open until someone succeeds to deposit these coatings by sputtering with impurity content of 100 ppm or less.

Coatings deposited by PVD should be also fully segregated nc-TiN/ Si_3N_4 nanocomposites because the decomposition of the solid solution occurs by diffusion in the bulk of the growing film for the following reasons: Based on the published values of the diffusion coefficient of Si in TiN, it has been estimated that about 100 s are needed for Si to diffuse over a distance of about 5 nm, which is taken as an approximate criterion for the segregation of the phases, whereas several 1000 s are needed at 300 °C (Veprek et al. 2006; Zhang and Veprek 2006). With the deposition rate of ≥ 1.5 nm/s used in our sputtering system (Prochazka et al. 2004), a 5 nm thick layer of the solid solution is deposited within about 3 s, whereas the time needed for Si to diffuse such distance is about 100 s. Therefore, homogeneous solid solution is formed at the surface of the growing films initially during the deposition, and the decomposition of the solid solution and phase segregation occurs by diffusion in the bulk. One often finds a suggestion that the ion bombardment may enhance the diffusion and phase segregation. However, at the high deposition rates, the decomposition of the solid solution by diffusion occurs in the bulk where the ion bombardment does not play any role. Moreover, ion bombardment will enhance mixing.

In the case of the coatings deposited by P-CVD, the deposition rate of 0.5–0.7 nm/s was only slightly lower. Therefore, there seems to be no rational reason why the mechanism of the decomposition of the solid solution and formation of the nanostructure should be different in P-CVD and PVD coatings. All the discrepancies regarding the morphology and achievable hardness appear to be associated with the impurity content.

2.5.2 The Possibility of the Formation of Superhard Nanocomposites in Other Systems

Based on our present understanding of the mechanism of hardness enhancement in the nc-TiN/ Si_3N_4 system, the following conditions are needed to achieve hardness enhancement by a factor of 3–5 as compared with the terminal phases which, of course, must be hard: (a) The system must be spinodal with a high de-mixing energy even if the segregated phases are not coherent, (b) the interfacial layer of the covalent XY compound must be stable between the surrounding TmN and another alternate hard material, (c) there must be some mechanism of strengthening of the interfacial XY layer similar to that in the nc-TiN/ Si_3N_4 nanocomposites, and (d) the material must be prepared with a sufficiently high purity.

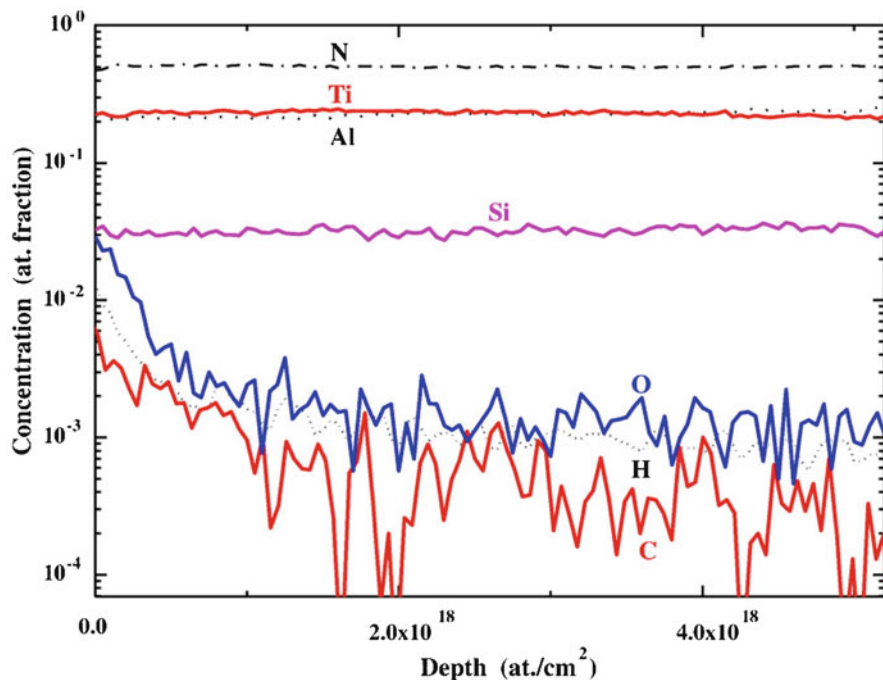


Fig. 6.15 Elastic recoil detection analysis (ERDA) of a typical nc-(Ti_{1-x}Al_x)N/Si₃N₄ coatings deposited by vacuum arc evaporation in an industrial coating system of the company SHM (SHM)

Thermodynamics

As shown in Fig. 6.9a, the superhard nc-TmN/Si₃N₄ nanocomposites have also been obtained with W₂N and VN. The company SHM is fabricating nc-(Ti_{1-x}Al_x)N/Si₃N₄ and nc-(Cr_{1-x}Al_x)N/Si₃N₄ nanocomposite coatings on tools that reach hardness of about 40 GPa when the oxygen impurity content is ≤ 1000 ppm (see Fig. 6.15). The lowest impurity content that has been achieved so far in such coatings deposited in an industrial coating equipment of the SHM company was about 700 ppm [see Fig. 21 in Veprék (2013)]. Thus, an improvement of the impurity by a factor of 3–4 is needed to reach the hardness of ≥ 50 GPa in the industrially produced coatings.

As mentioned, all transition metal nitrides and Si₃N₄ are immiscible, and they should probably decompose by spinodal mechanism, provided the lattice parameters of the TmN and Si₃N₄ do not differ too much. In such case, the only limitation is the stability of the interracial fcc-Si₃N₄-like layer. When the lattice mismatch between the transition metal nitride and Si₃N₄ is too large, the decomposition will not be coherently spinodal.

Using a combined first-principle DFT calculation and thermodynamic modeling, our group has studied a limited number of possible systems. The results are briefly summarized here:

- The Zr-Si-N (Sheng et al. 2008) and Al-Si-N (Sheng et al. 2013) systems are not coherently spinodal and, therefore, should decompose by nucleation and growth without the formation of a sharp interfacial Si_3N_4 layer. Therefore, the hardness enhancement observed in these systems is due to grain refinement only.
- Also the Zr-Al-N system should decompose by nucleation and growth (Sheng et al. 2008), and as we shall see, the fcc-AlN interfacial layer is unstable with ZrN.
- The $\text{Ti}_{1-x}\text{B}_x\text{N}$ system consisting of stoichiometric TiN and BN is chemically spinodal, and superhard nc-TiN/1 ML-BN nanocomposites have been prepared by P-CVD (Karvankova et al. 2006), whereas the frequently reported nitrogen-deficient $\text{TiB}_x\text{N}_{1-x}$ (“TiN + TiB_x ”) system should decompose by nucleation and growth (Zhang et al. 2008). However, the large difference of the sizes of boron and titanium atoms makes a coherent or semi-coherent interfacial BN layer impossible to form [see Fig. 12a in Karvankova et al. (2006)]. Moreover, the 1 ML of fcc-BN between TiN slabs is unstable already at 0 K (Ivashchenko and Veprek 2013). Therefore, the hardness enhancement observed in the nc-TiN/BN nanocomposites is most probably due to the “strongest size,” as seen in Fig. 6.16. The maximum hardness of about 50 GPa is achieved in this system when the surface coverage of the TiN nanocrystals by BN reaches about 1 ML as in the nc-TiN/ S_3N_4 system. Moreover, the electronegativity of boron (2.0) is slightly larger than that of silicon (1.8). Therefore, one might believe that the mechanism of the hardness enhancement is similar in both systems. This is however not the case because due to the large misfit between TiN and BN, there are also some Ti-B bonds even at the maximum hardness and 1 ML coverage of TiN nanocrystals with BN (Karvankova et al. 2006). By careful observation (Fig. 6.16), one sees that the maximal hardness correlates with the size of the TiN nanocrystals around 10 nm, i.e., with “the strongest size.” Therefore, the hardness enhancement in these nanocomposites is only due to the refinement of the grain size but not due to a “strengthened” interfacial layer.
- This example should be a warning that in many other systems, where a hardness enhancement up to 30–35 GPa has been found upon possible formation of nanocomposites, it was probably solely due to the grain refinement.
- One of the most promising systems is Zr-Al-O because it is chemically spinodal (Sheng et al. 2011a, b) and should have an “infinite oxidation resistance” which is very important in many industrial applications. However, because the hard corundum $\alpha\text{-Al}_2\text{O}_3$ modification forms only at high temperatures of ≥ 1000 °C, the mixed $\alpha\text{-(Al}_{1-x}\text{Cr}_x)_2\text{O}_3\text{-ZrO}_2$ and in particular $\text{Cr}_2\text{O}_3\text{-ZrO}_2$ systems may be more suitable to form hard and superhard nanocomposites. The formation of “Cr-Zr-O” coatings with a pronounced hardness enhancement has been achieved by M. Jilek from the SHM company (Jilek 2012).

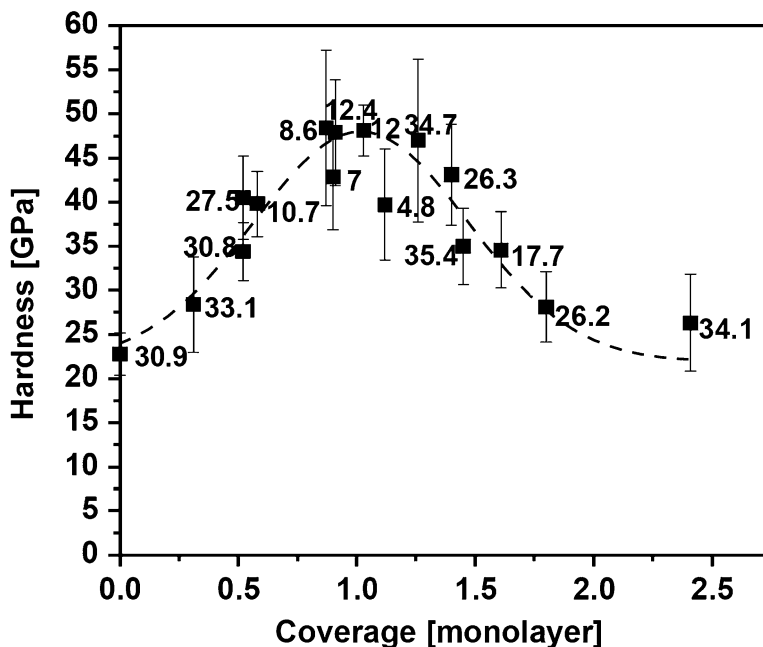


Fig. 6.16 Hardness of nc-TiN/BN nanocomposite coatings vs. surface coverage of the TiN nanocrystals with BN. The numbers are the corresponding size of the TiN nanocrystals (From Karvankova et al. (2006) with permission)

These limited examples clearly show that not all the systems can form superhard nanocomposites with hardness enhancement above 40–50 GPa because the interfacial covalent XY layer is not sharp and not strengthened. The most likely mechanism of the strengthening reported in many papers is due to refinement of the crystallite size. This is most probably valid also for papers reporting on nc-TmN/SiN_x nanocomposites with oxygen impurities of ≥ 0.3 –0.4%. The combined DFT and thermodynamics studies should be extended to other candidate systems because they are much faster and cheaper than the experimental trial and error approach.

Stability of the Interfacial Si₃N₄ and Alternate XY Layers

There are several ways of how to investigate the stability of the interfacial layer. The DFT method, which yields result at 0 K, does not guarantee that the structure obtained by structural relaxation until a minimum of the total energy has been achieved is really stable. Therefore, one has to study the dynamical phonon stability or artificially distort that structure and observe whether the total energy increases (the structure is stable or metastable in such a case) or decreases, in which case the

structure is unstable. Both approaches have been used to study the stability of the 1 ML-fcc-SiN layers pseudomorphically stabilized between TiN slabs. The artificial distortion approach has been used by Zhang et al. who showed that the fcc-(111)- and fcc-(110)-TiN interfacial monolayers are stable, but the fcc-(001)-SiN one is unstable. However, it has been stabilized by distortion of the Si atoms in (Veprek et al. 2004b) direction by 12 %, where the Si is essentially only fourfold coordinated (Zhang et al. 2009a, b). Marten et al. (2010) conducted the dynamic phonon studies of this system and confirmed the results of Zhang et al. More recently, Ivashchenko et al. used QMD to study this system at high temperatures and confirmed also these results (Ivashchenko et al. 2012). Interestingly, in the QMD calculations of Ivashchenko et al., the distortion of the Si atoms within the 1 ML SiN was random and not regular in the (Veprek et al. 2004b) direction as in the DFT studies of Zhang et al. This is due to the fact that the random distribution decreases the elastic lattice strain and concomitant elastic energy. This is seen as a decrease of the total energy after “annealing” the system to high temperature and “cooling” down to 300 K in a simulated “experiment.”

The probably most efficient method is the phonon study of the soft modes, as recently done by Ivashchenko et al. [Ivashchenko et al. (2014); Ivashchenko and Veprek (2013)]. When the structure is stable with respect to a given phonon mode, its phonon vector is real, i.e., small distortions of the atoms from their equilibrium positions are damped. When, however, the structure is unstable upon an infinitesimal deformation corresponding to the given phonon mode that is driving the structural transformation, that phonon will be amplified which shows imaginary phonon vector (Dove 1993). Conventionally, this situation is represented by negative phonon frequencies.

Figure 6.17a shows the frequencies of soft phonon $\Lambda_3[2\pi/a(1/8,1/8,1/8)]$ and $\Delta_5[2\pi/a(1/4,0,0)]$ modes of the B1-AlN interfacial layer as the function of lattice parameters of the surrounding transition metal nitride slabs (Ivashchenko et al. 2014). The frequencies are positive for lattice parameters < 0.44 nm, i.e., an interfacial AlN layer should be stable between the slabs of corresponding nitrides such as TiN, VN, NbN, and the like but unstable, e.g., with ZrN whose lattice parameter is close to 0.47 nm.

However, it remains an open question if one could prepare superhard nanocomposites with a large hardness enhancement in the systems Ti-Al-N, V-Al-N, and Nb-Al-N because although some of them are chemically spinodal, the de-mixing energy is the order of magnitude smaller than that in the Ti-Si-N system, as shown, e.g., for the Ti-Al-N (Zhang and Veprek 2007a) and Cr-Al-N (Zhang and Veprek 2007b) systems. Furthermore, the electronegativity of Al (1.5) is similar or even lower than that of the transition metals mentioned (Ti-1.5, V-1.6, Nb-1.6). Thus, a strengthening of the fcc-AlN interfacial monolayer by valence charge transfer is ruled out. Therefore, superhard nc-TiN/AlN and related nanocomposites with a similar hardness enhancement mechanism as in the nc-TiN/Si₃N₄ system are unlikely to form.

In a similar way, it was shown that fcc-BN interfacial monolayer is unstable for lattice parameter of the TmN larger than about 0.32 nm [see Fig. 1 in Ivashchenko

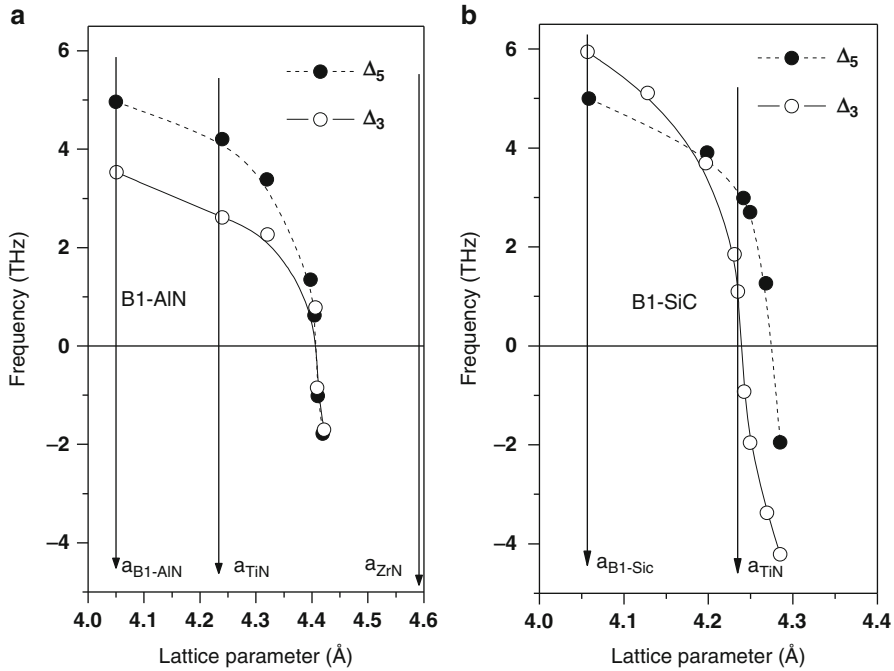


Fig. 6.17 (a) Frequencies of soft phonon $\Delta_3[2\pi/a(1/8,1/8,1/8)]$ and $\Delta_5[2\pi/a(1/4,0,0)]$ modes of B1-AIN interfacial layer and (b) for B1-SiC interfacial monolayer as function of lattice parameters of the surrounding transition metal nitride slabs (From Ivashchenko et al. (2014) and Ivashchenko and Veprek (2013) with permission)

and Veprek (2013)] which lends a further support to the fact that the hardness enhancement observed in the nc-TiN/BN nanocomposites is simply due to refinement of the grain sites of the TiN, as discussed above.

Interesting is the question if one could use SiC as the interfacial layer because Kong et al. reported significant hardness enhancement in TiN/SiC heterostructures deposited by magnetron sputtering at room temperature with TiN slabs of 4.3 nm and SiC layers of 0.6 nm thickness (Kong et al. 2007). Figure 6.17b shows the phonon frequencies of 1 ML fcc-SiC layer between TmN slabs of different lattice parameters. The lattice parameter of TiN of 0.423 nm is just close to the instability by the soft modes. Therefore, upon heating to 600 K, the fcc-SiC interfacial layer becomes unstable and converts to a disordered structure with broken bonds [see Fig. 3 in Ivashchenko and Veprek (2013)]. Moreover, $\text{TiN}_{1-x}\text{C}_x$ forms stable substitutional solid solution where carbon atoms replace nitrogen. In $\text{TiN}_{1-x}\text{C}_x$ deposited by P-CVD at temperature of 560 °C, with increasing fraction of carbon, the hardness increases from that of TiN to that of TiC following the rule of mixtures [see Fig. 8 in Veprek et al. (1996)]. Therefore, even when the TiN/SiC heterostructures deposited at room temperature have shown an interesting hardness enhancement, nc-TiN/SiC nanocomposites cannot be prepared because this system forms a stable solid solution.

In summary to this section, the understanding available to us now suggests that superhard nanocomposites with hardness enhancement by a factor of 3–5 can be formed only in the Tm-Si-N systems where the lattice parameter of the transition metal nitride does not differ too much from that of SiN_x , because only such systems are spinodal with large de-mixing energy, and the interfacial 1 ML SiN_x with silicon fourfold bonded to nitrogen is stable and strengthened by valence charge transfer. In majority of nanocomposites, where some hardness enhancement has been reported, this was due to a simple refinement of the grain size toward the “strongest size.”

3 Industrial Applications

As already mentioned, the nc-($\text{Ti}_{1-x}\text{Al}_x$)N/ Si_3N_4 nanocomposites have been pioneered as wear-protection coatings on tools for machining by Czech company SHM since 1996, followed soon by many other companies. The advantage of the nanocomposites is not only the higher hardness which reduces the abrasion wear but also (an in many cases mainly) their higher oxidation resistance up to above 900 °C, which is about three times better than that of the ($\text{Ti}_{1-x}\text{Al}_x$)N coatings, and therefore reduces the chemical wear by oxidation. The nc-($\text{Cr}_{1-x}\text{Al}_x$)N/ Si_3N_4 nanocomposites show even better oxidation resistance above 1000 °C [see Fig. 10 in Cselle (2005)]. We refer to our reviews for further details and information (Veprek and Veprek-Heijman 2008; Veprek 2013). Here we only emphasize several important points and give some examples of more recent achievements.

The high oxidation resistance is very important because in many machining operations, such as drilling, the cutting edge is running almost dry even when coolants are used. Thus, the number of holes being drilled by drills coated with the nc-($\text{Ti}_{1-x}\text{Al}_x$)N/ Si_3N_4 nanocomposites is more than factor of 3 larger than that with the conventional ($\text{Ti}_{1-x}\text{Al}_x$)N coatings. Moreover, if one can reduce the amount of coolant or even eliminate them in dry machining, one can significantly reduce the overall costs of the machining by up to 30 %.

Besides the high hardness, the nanocomposites also show a very high elastic limit of almost 10 %, which means that they sustain large strain without formation of cracks [see Fig. 9 in Veprek et al. (2003)]. This is particularly important in interrupted cutting, such as milling. However, the “harder” machining and longer lifetime of tool coated with these coatings may result in fatigue of the material of which the tools are made as illustrated by curve 3 in Fig. 6.18. Because the mills coated with the nanocomposites allowed longer lifetime of the tools, fatigue in the cemented carbide of which the tool has been made of caused an unpredictable sudden wear. Such behavior cannot be tolerated because the operator must know when to change the tool to avoid damage to the part being machined. The solution was the TripleCoatings[®] with about 2 μm thick underlayer of ($\text{Ti}_{1-x}\text{Al}_x$)N and about 1 μm top layer of the nc-($\text{Ti}_{1-x}\text{Al}_x$)N/ Si_3N_4 nanocomposites (Cselle 2008). In such a way, the wear became predictable and the lifetime of the tool has been

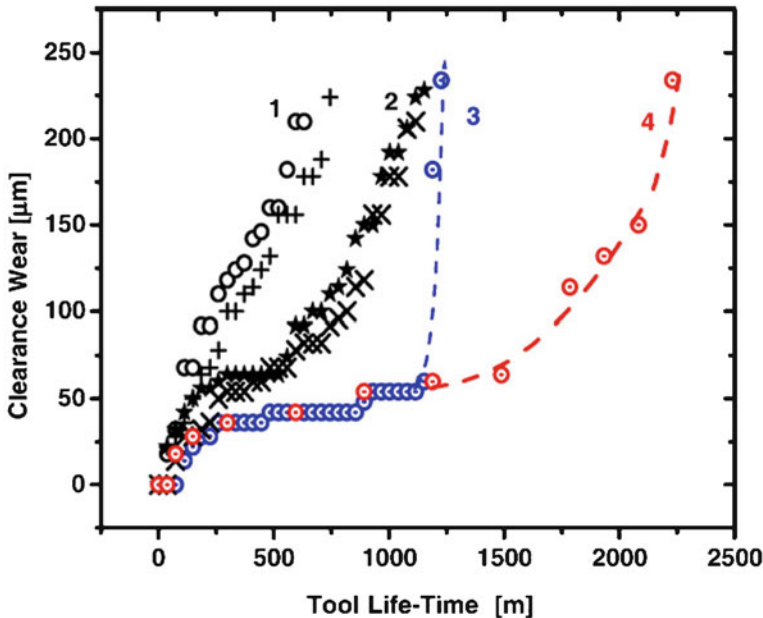
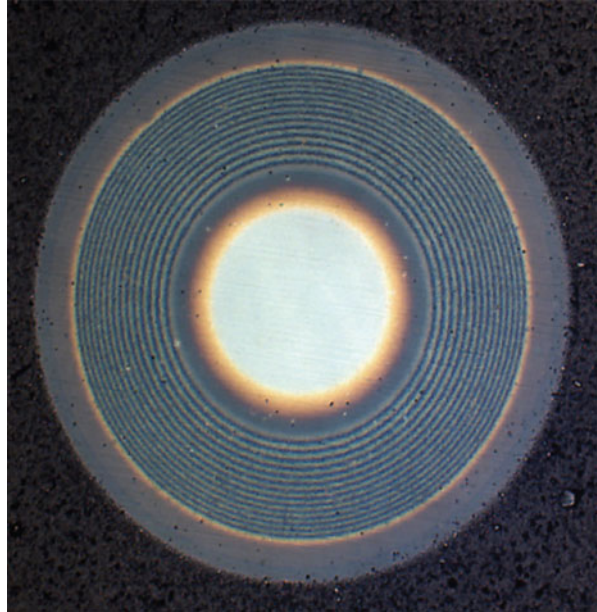


Fig. 6.18 Milling of 56 HRC hard steel using end mills made of cemented carbide coated with different coatings: 1, conventional $(\text{Ti}_{1-x}\text{Al}_x)\text{N}$ coatings from two different manufacturers; 2, “TiSiN” coatings from a foreign company; 3, nc- $(\text{Ti}_{1-x}\text{Al}_x)\text{N}/\text{Si}_3\text{N}_4$ nanocomposite coatings; and 4, “TripleCoatings[®]” consisting of about 2 μm thick $(\text{Ti}_{1-x}\text{Al}_x)\text{N}$ border layer and 1 μm thick nc- $(\text{Ti}_{1-x}\text{Al}_x)\text{N}/\text{Si}_3\text{N}_4$ nanocomposite *top* layer (From Cselle (2005) with permission)

increased by almost a factor of 5 as compared with the conventional $(\text{Ti}_{1-x}\text{Al}_x)\text{N}$ coatings (curve 4 in Fig. 6.18). One can also see that the nc- $(\text{Ti}_{1-x}\text{Al}_x)\text{N}/\text{Si}_3\text{N}_4$ nanocomposites are significantly better than the nc-TiN/ Si_3N_4 ones (curve 2 in Fig. 6.18), probably because of higher oxidation resistance of the former.

The low thermal conductivity of the nanocomposites reduces the flow of heat released due to the machining into the cutting edge. The low thermal conductivity is caused by intense phonon scattering on the grain boundaries of the 3–4 nm small nanocrystals. In the case of “TiSiN” nanocomposite coatings, the thermal conductivity decreased from about 12 W/m · K for TiN to about 1.7 W/m · K for TiSiN nanocomposite coatings with high Si content. For the Al + Si content where the hardness of the coatings reached maximum, the thermal conductivity was about 3 W/m · K (Samani et al. 2013). The thermal conductivity increases with increasing temperature. The lowest thermal conductivity and its lowest increase with temperature have been found for the CrAlSiN nanocomposites (Martan and Benes 2012). A significant decrease of the thermal conductivity has been reported also for TiN/TiAlN multilayers (Samani et al. 2015). The low thermal conductivity of the nanocomposite coatings is of particular interest for tools made of HSS which must not be heated above 530 °C because above that temperature it softens.

Fig. 6.19 Calotec in the coatings of the indexable inserts used for the milling of rails for fast trains showing the depth profile: substrate (cemented carbide) in the center and adhesion TiN layer (the first red-yellow layer), followed by a multilayers consisting of $(\text{Ti}_{1-x}\text{Al}_x)\text{N}$ (dark) and TiN (red yellow) with top layer of the nc- $(\text{Ti}_{1-x}\text{Al}_x)\text{N}/\text{Si}_3\text{N}_4$ nanocomposite (From Pramet SHM (2014) with permission)



Fast trains, such as Shinkansen in Japan, TGV in France, ICE in Germany, and others, are running at a speed of more than 300 km/h. In that case, the roughness of the rails must be less than 0.2 mm to avoid not only uncomfortable tremors and vibration of the train and noise but also to reduce the wear and possible crack formation in the rails. Therefore, the rails have to be periodically machined by milling. The tool has typically a diameter of about 60 cm and 22 teeth with many indexable inserts fixed there. It operates at 120–150 revolutions per minute with a surface speed of 220–280 m/min and feed of 700 m/h. The machining can be done only in the night when the fast trains do not operate. The company SHM in collaboration with the manufacturer of the indexable inserts Pramet developed special coatings shown in Fig. 6.19 (Pramet SHM 2014). The calotec ground section shows the depth profile of the coating: substrate (cemented carbide) in the center and adhesion TiN layer (the first red-yellow layer), followed by a multilayer consisting of $(\text{Ti}_{1-x}\text{Al}_x)\text{N}$ (dark) and TiN (red yellow) with top layer of the nc- $(\text{Ti}_{1-x}\text{Al}_x)\text{N}/\text{Si}_3\text{N}_4$ nanocomposite. This coating enabled to increase the lifetime of the expensive tool by more than 20 % and in such a way to extend the length of the rail that can be machined with one tool to more than 2 km.

As last example, we show in Fig. 6.20 tools made of steel for injection molding of Al alloys in fabrication of parts for automotive industry, after the fabrication of 15,000 parts. The tool treated in a conventional way by nitriding (left) shows a clear wear and had to be exchanged, whereas the tool coated with 2–3 μm thick nc- $(\text{Cr}_{1-x}\text{Al}_x)\text{N}/\text{Si}_3\text{N}_4$ coating does not show any noticeable wear. Obviously, the nanocomposites offer a great advantage also in operation where a combined abrasive and chemical wear occurs.



Fig. 6.20 Tools for injection molding of Al alloys in fabrication of parts for automotive industry, both after the fabrication of 15,000 parts. The length and diameter of the tools are about 200 and 20 mm, respectively. *Left tool* with conventional surface treatment by nitriding, *right tool* coated with 2–3 μm thick nc-($\text{Cr}_{1-x}\text{Al}_x$)N/Si₃N₄ coating [From SHM, private communication (2013)]

4 Conclusions

The search for new intrinsically super- and ultrahard materials should not consider only the high values of elastic moduli, but it has to study in detail the electronic stability upon large shear and the deformation paths. The presently available results show that materials which contain d-metals or non-binding electron pairs are likely to undergo electronic instability and transformation to other phases with low plastic resistance. Thus, diamond will probably remain the intrinsically hardest material.

More promising are attempts to design extrinsically superhard nanostructured materials, such as heterostructures, nanosized materials with crystallite size close to 10–15 nm (the “strongest size”) and in particular nanostructured materials with low-energy grain boundaries. The recently prepared nanotwinned nt-c-BN and t-diamond reached the load-invariant hardness of 109 and 200 GPa, respectively.

Super- and ultrahard nanocomposites with strengthened interfacial layer, such as nc-TiN/Si₃N₄ and nc-TiN/Si₃N₄/TiSi₂, can reach hardness in excess of

100 GPa provided they are correctly prepared with low impurity content. The nc-(Ti_{1-x}Al_x)N/Si₃N₄ and nc-(Cr_{1-x}Al_x)N/Si₃N₄ coatings are used as wear-protection coatings on tools for machining, stamping, forming, injection molding, and the like. Their advantage is not only the higher hardness but also high oxidation resistance and resistance against chemical corrosion as compared to their conventional counterparts (Ti_{1-x}Al_x)N and (Cr_{1-x}Al_x)N.

We have also shown that not all “nanocomposites” reported in many publications during the last two decades can be superhard. In many cases, the observed, relatively small increase of the hardness was due to simple refinement of the grain size. The conditions needed for achieving the high hardness of ≥ 100 GPa in nanocomposite systems have been discussed in some detail, and some promising systems have been identified and others ruled out.

Acknowledgment We would like to thank Company SHM for the financial support of our work and the Department of Chemistry of the Technical University of Munich for providing us the space and access to the computer facilities.

References

- Argon AS (2008) Strengthening mechanisms in crystal plasticity. Oxford University Press, Oxford
- Argon AS, Yip S (2006) The strongest size. *Philos Mag Lett* 86:713–720
- Auciello O (2010) Microchip-embedded capacitors for implantable neural stimulators. In: Zhou DD, Greenbaum E (eds) *Implantable neural prostheses 2, Techniques and engineering approaches*. Springer, New York
- Auciello O, Shi B (2010) Science and technology of bio-inert thin films as hermetic-encapsulating coatings for implantable biomedical devices: application to implantable microchip in the eye for the artificial retina. In: Zhou DD, Greenbaum E (eds) *Implantable neural prostheses 2, Techniques and engineering approaches*. Springer, New York
- Barna PB, Adamik M (1998) Fundamental structure forming phenomena of polycrystalline films and structure zone models. *Thin Solid Films* 317:27–33
- Barnett SA (1993) Deposition and mechanical properties of superlattice thin films. In: Fracombe MH, Vossen JL (eds) *Physics of thin films vol. 17 mechanic and dielectric properties*. Academic, Boston
- Barnett SA, Madan A (1998) Superhard superlattices. *Phys World* 11:45–48
- Bläß UW, Baruskova T, Schwarz MR, Köhler A, Schimpf C, Petruscha IA, Mühle U, Rafaja D, Kroke E (2015) Bulk titanium nitride ceramics – significant enhancement of hardness by silicon nitride addition, nanostructuring and high pressure sintering. *J Eur Ceram Soc* 35:2733–2744
- Bringa EM, Rosolankova K, Rudd RE, Remington BA, Wark JS, Duchaineau M, Kalantar DH, Hawreliak J, Belaket J (2006) Shock deformation of face-centred-cubic metals on subnanosecond timescales. *Nat Mater* 5:805–809
- Christiansen S, Albrecht M, Strunk HP, Veprek S (1998) Microstructure of novel superhard nanocrystalline-amorphous composites as analyzed by high resolution transmission electron microscopy. *J Vac Sci Technol B* 16:19–22
- Chu X, Barnett SA (1995) Model of superlattice yield stress and hardness enhancement. *J Appl Phys* 77:4403–4411

- Chung H-Y, Weinberger MB, Levine JB, Kavner A, Yang JM, Tolbert SH, Kaner RB (2007) Synthesis of ultra-incompressible superhard rhenium diboride at ambient pressure. *Science* 316:436–439
- Cohen ML (1994) Predicting properties and new materials. *Solid State Commun* 92:45–52
- Cselle T (2005) Application of coatings for tooling: Quo Vadis 2005? Vacuum's Best, Special issue of the German journal: *Vakuum in Forschung und Praxis*. Wiley, Weinheim, p 33
- Cselle T (2008) TripleCoatings[®] – a new generation of PVD-coatings for machining tools. In: Weinert K (ed) *Spanende Fertigung*, 5. Auflage. Vulkan-Verlag, Essen, pp 258–268, in German
- Dove MT (1993) *Introduction to lattice dynamics*. Cambridge University Press, Cambridge
- Dub SN, Petrusha IA (2006) Mechanical properties of polycrystalline c-BN obtained from pyrolytic g-BN by direct transformation technique. *High Press Res* 26:71–77
- Dubrovinskaia N, Solozhenko VL, Miyajima N, Dimitriev V, Kurakevych OO, Dubrovinsky L (2007) Superhard nanocomposite of dense polymorphs of boron nitride: noncarbon material has reached diamond hardness. *Appl Phys Lett* 90:101912-1-3
- Erdemir A, Eryilmaz OL, Urgen M, Kazmanli K, Mehta N, Prorok B (2005) Tribology of nanostructured materials and coatings. In: Gogotsi Y (ed) *Handbook of nanomaterials*. CRC Publication, Boca Raton, pp 685–711
- Eremets MI, Trojan IA, Gwaze P, Huth J, Boehler R, Blank VD (2005) The strength of diamond. *Appl Phys Lett* 87:141902-1-3
- Eriksson AO, Tengstrand O, Lu J, Jensen J, Eklund P, Rosén J, Petrov I, Greene JE, Hultman L (2014) Si Incorporation in $Ti_{1-x}Si_xN$ films grown on TiN(001) and (001)-faceted TiN(111) columns. *Surf Coat Technol* 257:121–128
- Field JE (ed) (1992) *The properties of natural and synthetic diamond*. Academic, San Diego
- Flink A, Larsson T, Sjölen J, Karlsson L, Hultman L (2005) Influence of Si on the microstructure of arc evaporated (Ti, Si)N thin films: evidence for cubic solid solutions and their thermal stability. *Surf Coat Technol* 200:1535–1542
- Flink A, Beckers M, Sjölen J, Larsson M, Braun S, Karlsson L, Hultman L (2009) The location and effects of Si in $(Ti_{1-x}Si_x)N_y$ thin films. *J Mater Res* 24:2483–2498
- Gao F, He J, Wu E, Liu S, Yu D, Li D, Zhang S, Tian Y (2003) Hardness of covalent crystals. *Phys Rev Lett* 91:015502-1-4
- Gogotsi YG, Kailer A, Nickel KG (1999) Transformation of diamond to graphite. *Nature* 401:663–664
- Gottstein G (2004) *Physical foundations of material science*. Springer, Berlin
- Gruen DM (1999) Nanocrystalline diamond films. *Annu Rev Mater Sci* 29:211–259
- Hao S, Delley B, Veprek S, Stampfl C (2006a) Superhard nitride-based nanocomposites: role of interfaces and effect of impurities. *Phys Rev Lett* 97:086102-1-4
- Hao S, Delley B, Stampfl C (2006b) Structure and properties of $TiN(111)/Si_xN_y/TiN(111)$ interfaces in superhard nanocomposites: first-principles investigations. *Phys Rev B* 74:035402-1-12
- Helmersson U, Todorova S, Barnett SA, Sundgren JE (1987) Growth of single-crystal TiN/VN strained-layer superlattices with extremely high mechanical hardness. *J Appl Phys* 62:481–484
- Herr W, Broszeit E (1997) The influence of a heat treatment on the microstructure and mechanical properties of sputtered coatings. *Surf Coat Technol* 97:335–340
- Hill R (1950) *The mathematical theory of plasticity*. Oxford University Press, Oxford
- Hilz G, Holleck H (1996) Structure and effect of interfaces in $TiC-TiB_2-B_4C-SiC$ nanosized multilayer systems. *Int J Refract Metals Hard Mater* 14:97–104
- Holleck H, Schier V (1995) Multilayer PVD coatings for wear protection. *Surf Coat Technol* 76–77:328–336
- Hsieh MH, Tsai MH, Shen WJ, Yeh AW (2013) Structure and properties of two Al–Cr–Nb–Si–Ti high-entropy nitride coatings. *Surf Coat Technol* 221:118–123
- Huang PK, Yeh JW (2009) Effect of substrate temperature and post-annealing on microstructure and properties of $(AlCrNbSiTiV)N$ coatings. *Thin Solid Films* 518:180–184

- Huang Q, Yu D, Xu B, Hu W, Ma Y, Wang Y, Zhao Z, Wen B, He J, Liu Z, Tian Y (2014) Nanotwinned diamond with unprecedented hardness and stability. *Nature* 510:250–253
- Hubbard KM, Jervis TR, Mirkarimi PB, Barnett SA (1992) Mechanical properties of epitaxial TiN/(V_{0.5}Nb_{0.4})N superlattices measured by nanoindentation. *J Appl Phys* 72:4466–4468
- Ivashchenko VI, Veprek S (2013) First-principles molecular dynamics study of the thermal stability of the BN, AlN, SiC and SiN interfacial layers in TiN-based heterostructures: comparison with experiments. *Thin Solid Films* 545:391–400
- Ivashchenko VI, Veprek S, Turchi PEA, Shevchenko VI (2012) Comparative first-principles study of TiN/SiN_x/TiN interfaces. *Phys Rev B* 85:195403-1-15
- Ivashchenko VI, Veprek S, Turchi PEA, Shevchenko VI, Leszczynski J, Gorb L, Hill F (2014) First-principles molecular dynamics investigation of thermal and mechanical stability of the TiN(001)/AlN and ZrN(001)/AlN heterostructures. *Thin Solid Films* 564:284–293
- Ivashchenko VI, Veprek S, Argon AS, Turchi PEA, Gorb L, Hill F, Leszczynski J (2015) First-principles quantum molecular calculations of structural and mechanical properties of TiN/SiN_x heterostructures, and the achievable hardness of the nc-TiN/SiN_x nanocomposites. *Thin Solid Films* 578:83–92
- Jian WW, Cheng GM, Xu WZ, Yuan H, Tsai MH, Wang QD, Koch CC, Zhu YT, Mathaudhu SN (2013) Ultrastrong Mg alloy via nano-spaced stacking faults. *Mater Res Lett* 1:61–67
- Jilek M (2012) Private communication 2012, Unpublished
- Karvankova P, Männling HD, Eggs CH, Veprek S (2001) Thermal stability of ZrN–Ni and CrN–Ni superhard nanocomposite coatings. *Surf Coat Technol* 146–147:280–285
- Karvankova P, Veprek-Heijman MGJ, Azinovic D, Veprek S (2006) Properties of superhard nc-TiN/a-BN and nc-TiN/a-BN/a-TiB₂ nanocomposite coatings prepared by plasma induced chemical vapor deposition. *Surf Coat Technol* 200:2978–2989
- Koehler JS (1970) Attempt to design a strong solid. *Phys Rev B* 2:547–551
- Kong M, Dai J, Lao J, Li G (2007) Crystallization of amorphous SiC and superhardness effect in TiN/SiC nanomultilayers. *Appl Surf Sci* 253:4734–4739
- Lehoczyk SL (1978a) Retardation of dislocation generation and motion in thin-layered metal laminates. *Phys Rev Lett* 41:1814–1818
- Lehoczyk SL (1978b) Strength enhancement in thin-layered Al-Cu laminates. *J Appl Phys* 49:54795485
- Liu AY, Cohen ML (1989) Prediction of new low compressibility solids. *Science* 245:841–842
- Martan J, Benes P (2012) Thermal properties of cutting tool coatings at high temperatures. *Thermochim Acta* 539:51–55
- Marten T, Isaev EI, Alling B, Hultman L, Abrikosov IA (2010) Single-monolayer SiN_x embedded in TiN: a first-principles study. *Phys Rev B* 81:212102-1-4
- Matthews A, Jones R, Dowey S (2001) Modelling and deformation behaviour of multilayer coatings. *Tribol Lett* 11:103–106
- McClintock FA, Argon AS (1966) Mechanical behavior of materials. Addison-Wesley, Reading
- Mirkarimi PB, Hultman L, Barnett SA (1990) Enhanced hardness in lattice-matched single-crystal TiN/V_{0.6}Nb_{0.4}N superlattices. *Appl Phys Lett* 57:2654–2656
- Mirkarimi PB, Barnett SA, Hubbard KM, Jervis TR, Hultman L (1994) Structure and mechanical properties of epitaxial TiN/V_{0.3}Nb_{0.7}N(100) superlattices. *J Mater Res* 9:1456–1466
- Münz WD, Lewis DB, Hovsepian PE, Schönjahn C, Ehasarian A, Smith IJ (2001) Industrial scale manufactured superlattice hard PVD coatings. *Surf Eng* 17:15–27
- Musil J (2000) Hard and superhard nanocomposite coatings. *Surf Coat Technol* 125:322–330
- Musil J, Hruby H (2000) Superhard nanocomposites Ti_{1-x}Al_xN films prepared by magnetron sputtering. *Thin Solid Films* 365:104–109
- Musil J, Kadlec S, Vyskocil J, Valvoda V (1988) New results in D.C. reactive magnetron deposition of TiN_x films. *Thin Solid Films* 167:107–119
- Musil J, Zeman P, Dohnal P (2007) Ti-Si-N films with a high content of Si. *Plasma Process Polym* 4:S574–S578

- Nastasi M, Mayer JW, Hirvonen J (1996) Ion-solid interaction. Cambridge University Press, Cambridge
- Niederhofer A, Nesladek P, Männling HD, Moto K, Veprek S, Jilek M (1999) Structural properties, internal stress and thermal stability of nc-TiN/Si₃N₄, nc-TiN/TiSi_x and nc-(Ti_{1-x}Al_ySi_x)N superhard nanocomposite coatings reaching the hardness of diamond. Surf Coat Technol 120–121:173–178
- Ninomiya T (1978) Theory of melting, dislocation model I & II. J Phys Soc Jpn 44:263–271
- Otto F, Yang Y, Bei H, George EP (2013) Relative effect of enthalpy and entropy on the phase stability of equiatomic high-entropy alloys. Acta Mater 61:2628–2638
- Pélišson A, Parlinska-Wojtan M, Hug HJ, Patscheider J (2007) Microstructure and mechanical properties of Al–Si–N transparent hard coatings deposited by magnetron sputtering. Surf Coat Technol 202:884–889
- Petrov I, Barna PB, Hultman L, Greene JE (2003) Microstructural evolution during film growth. J Vac Sci Technol A 21:S117–S128
- Porter DA, Easterling KE (2001) Phase transformations in metals and alloys, 2nd edn, reprinted by Nelson Thomes Ltd, Cheltenham
- Pramet SHM (2014) Advanced PVD coatings for milling of rails. MM Prumyslove Spektrum 6:64–66 (in Czech)
- Prilliman SG, Clark SM, Alivisatos AP, Karvankova P, Veprek S (2006) Strain and deformation in ultra-hard nanocomposites nc-TiN/a-BN under hydrostatic pressure. Mater Sci Eng A 437:379–387
- Prochazka J, Karvankova P, Veprek-Heijman MGJ, Veprek S (2004) Conditions required for achieving superhardness of ≥ 45 GPa in nc-TiN/a-Si₃N₄ nanocomposites. Mater Sci Eng A 384:102–116
- Rogl P, Schuster JC (1992) Phase diagrams of ternary boron nitride and silicon nitride, ASM The Materials Information Society, Material Parks, Ohio
- Samani MK, Ding XZ, Amini S, Khosravian N, Cheong JY, Chen G, Tay BK (2013) Thermal conductivity of titanium aluminum silicon nitride coatings deposited by lateral rotating cathode arc. Thin Solid Films 537:108–112
- Samani MK, Ding XD, Khosravian N, Amin-Ahmadi B, Yang Y, Chene G, Neyts EC, Bogaerts A, Tay BK (2015) Thermal conductivity of titanium nitride/titanium aluminum nitride multilayer coatings deposited by lateral rotating cathode arc. Thin Solid Films 578:133–138
- Saxonian (2015) Homepage of the Saxonian Institute for surface mechanics <http://www.siomec.de/en/113/Nanotwinned+diamond+with+unprecedented+hardness>
- Schiøtz J, Jacobsen KW (2003) A maximum in the strength of nanocrystalline copper. Science 301:1357–1359
- Schiøtz J, Di Tolla FD, Jacobsen KW (1998) Softening of nanocrystalline metals at very small grain sizes. Nature 391:561–563
- Schmalzried H (1995) Chemical kinetics of solids. WCH Verlag, Weinheim
- Sheng SH, Zhang RF, Veprek S (2008) Phase stabilities and thermal decomposition in the Zr_{1-x}Al_xN system studied by *ab initio* calculation and thermodynamic modeling. Acta Mater 56:968–976
- Sheng SH, Zhang RF, Veprek S (2011a) Phase stabilities and decomposition mechanism in the Zr–Si–N system studied by combined *ab initio* DFT and thermodynamic calculation. Acta Mater 59:297–307
- Sheng SH, Zhang RF, Veprek S (2011b) Study of spinodal decomposition and formation of nc-Al₂O₃/ZrO₂ nanocomposites by combined *ab initio* density functional theory and thermodynamic modeling. Acta Mater 59:3498–3509
- Sheng SH, Zhang RF, Veprek S (2013) Decomposition mechanism of Al_{1-x}Si_xN_y solid solution and possible mechanism of the formation of covalent nanocrystalline AlN/Si₃N₄ nanocomposites. Acta Mater 61:4226–4236
- Shin M, Hultman L, Barnett SA (1992) Growth, structure and microhardness of epitaxial TiN/NbN superlattices. J Mater Res 7:901–911

SHM <http://www.shm-cz.cz>

- Siegel RW, Fougere E (1995) Mechanical properties of nanophase metals. *NanoStructured Mater* 6:205–216
- Simunek A (2009) Anisotropy of hardness from first principles: the cases of ReB_2 and OsB_2 . *Phys Rev B* 80:060103(R)-1-4
- Simunek A, Vackar J (2006) Hardness of covalent and ionic crystals: first-principle calculations. *Phys Rev Lett* 96:085501-1-4
- Skrovanek SD, Bradt RC (1979) Microhardness of a fine-grain-size Al_2O_3 . *J Amer Ceram Soc* 62:215–216
- Solozhenko VL, Andrault D, Fiquet G, Mezouar M, Rubie DC (2001) Synthesis of superhard cubic BC_2N . *Appl Phys Lett* 78:1385–1387
- Solozhenko VL, Kurakevych OO, Andrault D, Godec YL, Mezouar M (2009) Ultimate metastable solubility of boron in diamond: synthesis of superhard diamondlike BC_5 . *Phys Rev Lett* 102:015506-1-4
- Solozhenko VL, Kurakevych OO, Godec YL (2012) Creation of nanostructures by extreme conditions: high-pressure synthesis of ultrahard nanocrystalline cubic boron nitride. *Adv Mater* 24:1540–1544
- Sproul WD (1994) Multilayer, multicomponent, and multiphase physical vapor deposition coatings for enhanced performance. *J Vac Sci Technol A* 12:1595–1601
- Sproul WD (1996) Reactive sputter deposition of polycrystalline nitride and oxide superlattice coatings. *Surf Coat Technol* 86/87:170–176
- Sumiya H, Uesaka S, Satoh S (2000) Mechanical properties of high purity polycrystalline c-BN synthesized by direct conversion sintering method. *J Mater Sci* 35:1181–1186
- Tabor D (1951) *The hardness of metals*. At the Clarendon Press, Oxford
- Tang F, Gault B, Ringer SP, Martin P, Bendavid A, Cairney JM (2010) Microstructural investigation of Ti–Si–N hard coatings. *Scripta Mater* 63:192–195
- Teter MD (1998) Computational Alchemy: the search for new superhard materials. *Mater Res Soc Bull* 23:22–27
- Tian Y, Xu B, Yu D, Ma Y, Wang Y, Hang Y, Hu W, Tang C, Gao Y, Luo K, Zhao Z, Wang LM, Weng B, He J, Liu Z (2013) Ultrahard nanotwinned cubic boron nitride. *Nature* 493:385–388
- Tsai MH, Yeh JW (2014) High entropy alloys: a critical review. *Mater Res Lett* 2:107–123
- Veprek S (1999) The search for novel superhard materials. *J Vac Sci Technol A* 17:2401–2420
- Veprek S (2013) Recent search for new superhard materials: Go nano! *J Vac Sci Technol A* 31:050822-1-33
- Veprek S, Reiprich S (1995) Concept for the design of novel superhard coatings. *Thin Solid Films* 268:64–71
- Veprek S, Veprek-Heijman MGJ (2007) The formation and role of interfaces in superhard nc- $\text{Me}_n\text{N}/\text{a-Si}_3\text{N}_4$ nanocomposites. *Surf Coat Technol* 201:6064–6070
- Veprek S, Veprek-Heijman MGJ (2008) Industrial applications of superhard nanocomposite coatings. *Surf Coat Technol* 202:5063–5073
- Veprek S, Veprek-Heijman MGJ (2012) Limits to the preparation of superhard nanocomposites: impurities, deposition and annealing temperature. *Thin Solid Films* 522:274–282
- Veprek S, Iqbal Z, Sarott FA (1982) A thermodynamic criterion of the crystalline-to-amorphous transition in silicon. *Philos Mag* 45:137–145
- Veprek S, Weidmann J, Glatz F (1995) Plasma chemical vapor deposition and properties of hard C_3N_4 thin films. *J Vac Sci Technol A* 13:2914–2919
- Veprek S, Haussmann M, Reiprich S, Li S, Dian J (1996) Novel thermodynamically stable and oxidation resistant superhard coating materials. *Surf Coat Technol* 86–87:394–401
- Veprek S, Niederhofer A, Moto K, Bolom T, Männling HD, Nesladek P, Dollinger G, Bergmaier A (2000) Composition, nanostructure and origin of the ultrahardness in nc-TiN/ Si_3N_4 /TiSi₂ nanocomposites with $H = 80$ to ≥ 100 GPa. *Surf Coat Technol* 133–134:152–159

- Veprek S, Mukherjee S, Karvankova P, Männling HD, He JL, Moto K, Prochazka J, Argon AS (2003) Limits to the strength of super- and ultrahard nanocomposite coatings. *J Vac Sci Technol A* 21:532–544
- Veprek S, Männling H-D, Niederhofer A, Ma D, Mukherjee S (2004a) Degradation of superhard nanocomposites by built-in impurities. *J Vac Sci Technol B* 22:L6–L9
- Veprek S, Männling HD, Jilek M, Holubar P (2004b) Avoiding the high-temperature decomposition and softening of $(Al_{1-x}Ti_x)N$ coatings by the formation of stable superhard nc- $(Al_{1-x}Ti_x)N/a-Si_3N_4$ nanocomposite. *Mater Sci Eng A* 366:202–205
- Veprek S, Veprek-Heijman MGJ, Karvankova P, Prochazka J (2005a) Different approaches to superhard coatings and nanocomposites. *Thin Solid Films* 476:1–29
- Veprek S, Karvankova P, Veprek-Heijman MGJ (2005b) Possible role of oxygen impurities in degradation of nc-TiN/ Si_3N_4 nanocomposites. *J Vac Sci Technol B* 23:L17–L21
- Veprek S, Männling HD, Karvankova P, Prochazka J (2006) The issue of the reproducibility of deposition of superhard nanocomposites with hardness of ≥ 50 GPa. *Surf Coat Technol* 200:3876–3885
- Veprek S, Argon AS, Zhang RF (2007) Origin of the hardness enhancement in superhard nc-TiN/ $a-Si_3N_4$ and ultrahard nc-TiN/ $a-Si_3N_4/TiSi_2$ nanocomposites. *Philos Mag Lett* 87:955–966
- Veprek S, Argon AS, Zhang RF (2010) Design of ultrahard materials: Go nano! *Philos Mag* 90:4101–4115
- Veprek-Heijman MGJ, Veprek RG, Argon AS, Parks DM, Veprek S (2009) Non-linear finite element constitutive modeling of indentation into super- and ultrahard materials: the plastic deformation of the diamond tip and the ratio of hardness to tensile yield strength of super- and ultrahard nanocomposites. *Surf Coat Technol* 203:3385–3391
- Xu B, Tian Y (2015) Ultrahardness: measurement and enhancement. *J Phys Chem* 119:5633–5638
- Yashar PC, Sproul WD (1999) Nanometer scale multilayered hard coatings. *Vacuum* 55:178–190
- Yashar PC, Barnett SA, Hultman L, Sproul WD (1999) Deposition and mechanical properties of polycrystalline Y_2O_3/ZrO_2 superlattices. *J Mater Res* 9:3614–3622
- Yip S (1998) The strongest size. *Nature* 391:532–533
- Zeman P, Cerstvy R, Mayrhofer PH, Mitterer C, Musil J (2000) Structure and properties of hard and superhard Zr-Cu-N nanocomposite coatings. *Mater Sci Eng A* 289:189–197
- Zhang RF, Veprek S (2006) On the spinodal nature of the phase segregation and formation of stable nanostructure in the Ti–Si–N system. *Mater Sci Eng A* 424:128–137
- Zhang RF, Veprek S (2007a) Metastable phases and spinodal decomposition in $Ti_{1-x}Al_xN$ system studied by *ab initio* and thermodynamic modeling, a comparison with the TiN– Si_3N_4 system. *Mater Sci Eng A* 448:111–119
- Zhang RF, Veprek S (2007b) Phase stabilities and spinodal decomposition in the $Cr_{1-x}Al_xN$ system studied by *ab initio* LDA and thermodynamic modeling: comparison with the $Ti_{1-x}Al_xN$ and TiN/ Si_3N_4 systems. *Acta Mater* 55:4615–4624
- Zhang RF, Veprek S (2008) Phase stabilities of self-organized nc-TiN/ $a-Si_3N_4$ nanocomposites and of $Ti_{1-x}Si_xN_y$ solid solutions studied by *ab initio* calculation and thermodynamic modeling. *Thin Solid Films* 516:2264–2275
- Zhang Y, Hong S, Chen C (2004) Superhard cubic BC_2N compared to diamond. *Phys Rev Lett* 93:195504-1-4
- Zhang Y, Hong S, Chen C (2006) Strain dependent bonding in solid C_3N_4 : high elastic moduli but low strength. *Phys Rev B* 73:064109-1-4
- Zhang RF, Sheng SH, Veprek S (2008) Stability of Ti–B–N solid solutions and the formation of nc-TiN/ $a-BN$ nanocomposites studied by combined *ab initio* and thermodynamic calculations. *Acta Mater* 56:4440–4449
- Zhang RF, Veprek S, Argon AS (2009a) Effect of nanometer-sized grains on the superhardness of $c-BC_5$: a first-principles study. *Phys Rev B* 80:233401-1-4
- Zhang RF, Argon AS, Veprek S (2009b) Friedel oscillations are limiting the strength of superhard nanocomposites and heterostructures. *Phys Rev Lett* 102:015503-1-4

- Zhang RF, Argon AS, Veprek S (2009c) Electronic structure, stability, and mechanism of the decohesion and shear of interfaces in superhard nanocomposites and heterostructures. *Phys Rev B* 79:245426-1-13
- Zhang RF, Legut D, Niewa R, Argon AS, Veprek S (2010a) Shear-induced structural transformation and plasticity in ultraincompressible ReB_2 limit its hardness. *Phys Rev B* 82:104104-1-7
- Zhang RF, Argon AS, Veprek S (2010b) Understanding why the thinnest SiN_x interface in transition-metal nitrides is stronger than the ideal bulk crystal. *Phys Rev B* 81:245418-1-7
- Zhang RF, Lin ZJ, Zhao YS, Veprek S (2011) Superhard materials with low elastic moduli: three-dimensional covalent bonding as the origin of superhardness in B_6O . *Phys Rev B* 83:092101-1-4
- Zhang RF, Legut D, Wen XD, Veprek S, Rajan K, Lookman T, Mao HK, Zhao YS (2014) Bond deformation paths and electronic instabilities of ultraincompressible transition metal diborides: case study of OsB_2 and IrB_2 . *Phys Rev B* 90:094115-1-6
- Zhao B, Gottstein G, Shvindlerman LS (2011) Triple junction effects in solids. *Acta Mater* 59:3510–3518
- Zhao B, Ziemons A, Shvindlerman LS, Gottstein G (2012) Surface topology and energy of grain boundary triple junctions in copper tricrystals. *Acta Mater* 60:811–818
- Zhu T, Li J, Ogata S, Yip S (2009) *MRS Bull* 34:167–172